El Niño-Southern Oscillation (ENSO) Signal in an Ice Core from Huascarán, Peru, 1994-2019

Research Thesis

Presented in Partial Fulfillment of the Requirements for graduation

"with Honors Research Distinction in Geography" in the undergraduate colleges of

The Ohio State University

By

Laurel Bayless

The Ohio State University

May 2021

Project Advisors: Professor Ellen Mosley-Thompson, Department of Geography

and Professor Lonnie Thompson, School of Earth Sciences

Abstract

This project investigates potential signatures of El Niño-Southern Oscillation (ENSO) as identified from analyses of an ice core from the col of Huascarán glacier (9.1ºS, 77.6ºW, 6050 m asl) in northern Peru. A reliable chemical signature of ENSO preserved in the ice offers the potential to extend the ENSO history beyond modern climatological observations. Knowledge of the history of ENSO will advance our understanding of modern climatological variability in ENSO patterns and may provide insight into how ENSO may evolve in a warmer climate. Two ice cores were recovered to bedrock in 2019 on the col of Huascarán glacier in the Peruvian Andes by a team from the Byrd Polar and Climate Research Center. Variations in the annual concentrations of F^-, Cl^-, SO_4^{2-}, NO_3^-, Na^+, NH_4^+, K^+, Mg^{2+}, Ca^{2+}, MSA (methane sulfonic acid, $CH_3SO_3^-$), $\delta^{18}O$, δD, and net accumulation were compared for El Niño events (1997-1998, 2009-2010, and 2015-2016), La Niña events (1998-2000, 2007-2008, and 2010-2011), and the other more neutral years from 1994 to 2019 measured in the same core. Annual values of the chemical markers and net accumulation were compared with standardized indices of sea surface temperatures (SSTs) in specific regions of the Pacific and Pacific Oceans (e.g., NIÑO4, NIÑO3.4, and AMO, the Atlantic Multidecadal Oscillation). Modeled upper tropospheric temperatures at Huascarán were compared with both Pacific SSTs and the Huascarán records to explore possible mechanisms for the connections identified. Consistent with previous research, the strongest relationship exists for isotopic variations (between ^{18}O and ^{16}O and between ^2H and ^1H) and NIÑO4 SSTs ($r=0.68$ and $r=0.67$ for $\delta^{18}O$ and δD, respectively). Other ENSO indices also were significantly positively correlated with isotopic values. A significant negative correlation exists between NIÑO4 SSTs and net accumulation ($r=-0.451$, $p<0.05$). T-tests indicate depletion of sulfate during El Niño events. A significant relationship ($r=0.571$, $p<0.05$) exists between the AMO and dust concentration. A possible mechanism for this connection is suggested by the very strong correlation between upper tropospheric temperatures (200 and 500 mb) and central Pacific SSTs. Central Pacific SSTs could influence the upper tropospheric temperatures at Huascarán, which could in turn influence the isotopic ratios in the ice at Huascarán.

Contents

1. Introduction

Tropical glaciers in South America preserve important archives of past occurrences of El Niño-Southern Oscillation (ENSO). ENSO refers to the east-west variation in depth of the thermocline in the equatorial Pacific Ocean, and it is the climatological phenomenon with the largest short-term global impact other than the annual cycle (McPhaden et al., 2020). The warm and cold phases of this oscillation are respectively referred to as El Niño and La Niña. ENSO refers to the periodic shift in conditions in the tropical Pacific Ocean, where the Walker and Hadley circulation typically lead to the buildup of warm water in the Western Pacific, a tilted thermocline which becomes shallower across the Pacific from west to east, and a cold tongue of deep water upwelling in the eastern Pacific (McPhaden et al., 2020). During El Niño events, the thermocline becomes flatter throughout the Pacific, and upwelling ceases in the eastern Pacific, leading to a more even distribution of heat throughout the Pacific Ocean. La Niña, the other extreme of this oscillation, is a strengthened version of the typical climate conditions, with stronger-than-normal buildup of heat in the western Pacific. Changes in the Pacific Hadley circulation result in changes in the subtropical jet stream position and strength, leading to partially predictable global climatological shifts in El Niño and La Niña conditions. In many ways, El Niño and La Niña act as opposing events, but El Niño events tend to be shorter and stronger than La Niña events, and SST cold anomalies in La Niña events extend farther west than the warm anomalies in El Niño events. These two phases of the oscillation are not mirror images of each other (McPhaden et al., 2020).

ENSO has broad and far-reaching climatological consequences. El Niño years are known to be associated with particularly high levels of cryospheric melting in the Andes (Thompson et al., 2017), forest fires in Amazonia, Australia, and southwest North America (Fasullo et al., 2018), and other global climate consequences. The warm phase of ENSO is of particular importance today as these events can force changes in the climate system from which it is impossible to return without a long period of sustained cooler temperatures. For example, Thompson et al. (2017) explored the important role of El Niño events in the melting of Andean glaciers, and they found that the 2015-2016 El Niño produced greater ice wastage along the margin of the Quelccaya Ice Cap compared to the warming trend over the past 15 years. These El Niño years are also known to result in an increase in global CO_2 levels for diverse reasons. Due to climate change, therefore, any increase in frequency or intensity of El Niño events could be instrumental in any of several facets of the Earth's systems reaching a critical tipping point. Understanding past variability of ENSO may help to illuminate the possible patterns of evolution of this oscillation under a warmer climate.

Peruvian glaciers are of particular interest because they are in an area that is very strongly affected by ENSO. The Peruvian coast normally experiences upwelling, which usually ceases during El Niño (warm phase) events. This study focuses specifically on El Niño events as recorded at Nevado Huascarán in northern Peru, the tallest tropical glacier, and it builds on the last study of the glacier's ENSO signal from 1874-1993 (Henderson, 1996). The purpose of this project is to assess how ENSO is recorded in the Huascarán ice core, and it extends Henderson's study by incorporating an increased array of chemical tracers with the potential to track the ENSO signal and by expanding the record to include the most recent history (1994 to 2019). Insight to the record of ENSO at Huascarán could serve the dual purpose of helping to interpret ice core sections predating modern climatological observations and illuminating shifting climate patterns in the region related to ENSO.

1.1. ENSO evidence/signature in South American Ice Cores

Thompson et al.'s 1992 publication on inter-annual climate variability from tropical and subtropical ice cores (Quelccaya Ice Cap, Peru and Dunde, China) notes that ENSO is the largest signal in tropical ice cores after the yearly signal. There is no definitive time-scale for El Niño events, although they tend to occur every two to seven years. ENSO cannot be predicted through simple methods, although forecasts are often able to predict likelihoods of El Niño and La Niña events months in advance.

Ice cores from Huascarán are expected exhibit stronger relationships with ENSO than the Quelccaya Ice Cap because Huascarán is closer to the equator, in the zone of maximum ENSO impact (Thompson et al., 1992). Additionally, the climate signal is still well-preserved at Huascarán compared to lower elevation glaciers which are currently affected by seasonal melting (Thompson et al., 2017). Other glaciers from which ice cores have been recovered in South America are even farther south, even more distant from the zone of maximal ENSO impact. However, it is useful to compare the records from Huascarán to the Quelccaya Ice Cap in southern Peru which has been studied extensively from cores retrieved over the past 40 years. Figure 1 shows Huascarán and Quelccaya on a map of Peru. Records from Illimani and Sajama, Bolivia also supplement these records, even though they are farther south from the area of maximum impact from ENSO.

Figure 1: Map of Peru including Huascarán in the Cordillera Blanca and Quelccaya Ice Cap in the Cordillera Vilcanota.

1.1.1. Huascarán

Previous studies of the Huascarán ice record (9.1ºS, 77.6ºW, 6050 m asl) have relied upon cores drilled in 1993. This record goes back to the Last Glacial Stage (LGS) and

indicates temperatures 5° to 6°C cooler at this time (Thompson et al., 1995). The LGS is characterized by an increase in dust concentrations and more negative values of $\delta^{18}O$ indicating greater depletion of ^{18}O relative to ^{16}O, similar to typical LGS signatures in polar ice cores. Holocene conditions were established by around 10,000 BP. This record indicates that the Holocene was warmest from 8400 to 5200 years BP, after which conditions gradually cooled until the Little Ice Age, which was followed by a strong warming trend over the past two centuries.

Henderson et al. (1999) explored the Huascarán core's record of ENSO and found that there was little relationship between net accumulation on Huascarán and ENSO from 1874-1993, unlike the accumulation on Quelccaya, where net accumulation and ENSO are known to be linked. Huascarán receives most of its precipitation during the austral summer (wet season), and due to the "amount effect", the seasonal $\delta^{18}O$-temperature relationship was the reverse of that normally found at higher latitudes. That is, warmer temperatures do not correspond with a higher ratio between ^{18}O and ^{16}O on the seasonal timescale in the tropical Andes. Therefore, the isotopic ratio between ^{18}O and ^{16}O tends to be higher (less negative) during the austral winter. However, on longer time scales, they found a positive relationship between $\delta^{18}O$ and temperature. Relationships with El Niño were stronger when more minor events were removed, and a greater similarity with the Quelccaya ice cap record emerged when decadal averages were compared. They concluded that a similarity in tropical SST patterns may be indicative of climate responses in the interior of South America. Additionally, they found that ^{18}O enrichment was most significant when the peak of the Pacific warming occurred in the first half of the calendar year (wet season). They noted that there was no strong foreshadowing to Niño events in ice cores in the Andes, likely because the precipitation there was of Atlantic origin.

Henderson (1996) explored the magnitude of Atlantic temperature variation due to El Niño events and found that the magnitude of extremes of ENSO-like oscillations in the Atlantic were much smaller than those in the Pacific, and would have been insufficient to be the dominant cause of the levels of isotopic enrichment associated with warm ENSO events at Huascarán. However, in a later study, Henderson et al. (1999) examined the mechanism through which the influence of the Pacific SSTs reached Huascarán by splitting the Huascarán isotopic record into quasi-monthly values which were then compared with Pacific and Atlantic SSTs and other climate parameters. They found a significant connection between South Atlantic 500 mb zonal wind velocity anomalies and $\delta^{18}O$ at Huascarán, although wind is unlikely to be the sole agent of fractionation in the $\delta^{18}O$ signal. They suggested that the ENSO sequence begins with warming on the Peruvian coast and that it reaches the Atlantic basin though an "atmospheric bridge" associated with the weakening of the trade winds. Wind stress anomalies then follow a north-south dipole in their effects, leading to notable effects in 500 mb wind stress anomalies. A continental shift in heavy precipitation from the equatorial region toward the subtropical jets follows in both hemispheres, and the 500 mb winds weaken. ^{18}O enrichment consequentially follows in Andean snowfall. The peak of El Niño events comes, according to Henderson et al. (1999), when the trade winds relax and the tropical Atlantic reaches peak warmth. Then, the Intertropical Convergence Zone (ITCZ), which had shifted to the north, returns south. Rainy conditions return to Amazonia, and the snowfall at Huascarán suddenly becomes more depleted in ^{18}O; that is, the $\delta^{18}O$ value becomes more negative.

Henderson et al. (1999) suggested that the onset of the El Niño disturbance at Huascarán occurred at the point of greatest Pacific SST anomaly and was identifiable though isotopic enrichment. A reversal toward isotopic depletion followed 10-14 months after the isotopic enrichment associated with Nordeste drought. From this study, Henderson et al. (1999) concluded that ^{18}O enrichment (less negative $\delta^{18}O$) in the Amazon and therefore at Huascarán during El Niño events was likely related to a combination of warmer temperatures and lower rainfall.

1.1.2. Quelccaya

Paleoclimatological study of the Quelccaya Ice Cap (QIC) (13.93S, 70.83W, 5670 m asl) began in the 1970s. Thompson et al. (1984) found a substantial decrease in ice accumulation at QIC during El Niño years. The 1982-1983 thermal year, one of the strongest El Niño events in recent history, had accumulation 70% lower than the average over the previous seven years. This low accumulation was likely the result of the droughts which typically expand over southern Peru during El Niño events.

A later study (Thompson et al., 2013) explored the climate history preserved in this ice core at annual resolution back to 683 CE. During the Medieval Climate Anomaly, they found below average net accumulation, and more variable and enriched $\delta^{18}O$, indicative of a variable climate. This pattern is consistent with other South American paleoclimate records, such as a lake core from Laguna Pumacocha (Bird et al., 2011). During the Little Ice Age (~1450-1850 CE), Thompson et al. (1986) found lower $\delta^{18}O$ throughout the event but higher net accumulation early in the event and lower accumulation from 1681 CE onward. During the current warm period, $\delta^{18}O$ and net accumulation increased. Higher lake levels in Lake Titicaca before 1975 typically corresponded with higher accumulation on Quelccaya, but recently this has not been the case, as mass wasting has led to lower accumulation at Quelccaya but not to lower lake levels (Thompson et al., 2013). This long study of Quelccaya climate variation can help with the interpretation of the record at Quelccaya: $\delta^{18}O$ has been higher and net accumulation has been lower in warmer periods. The Quelccaya Southern Dome ice core $\delta^{18}O$ record had a correlation coefficient of 0.55 with NINO4 SSTs, the region found to have the strongest relationship. Using three-year averages this correlation increased to 0.61. Subsequently, it has been found that melting increases during El Niño years, which is particularly important as the 0º isotherm is approaching the Quelccaya summit (Thompson et al., 2017).

According to Vuille et al. (2003), Pacific SSTs are the dominant control on $\delta^{18}O$ variability at Quelccaya despite the fact that precipitation primarily comes from the Amazon and additionally despite precipitation and temperature effects on $\delta^{18}O$ sometimes work in opposition. This is because a warm Pacific typically leads to enhanced westerly flow over the tropical Andes. Hurley et al. (2019) investigated the possible factors governing the ENSO signal in the $\delta^{18}O$ record on Quelccaya, including precipitation and temperature at Quelccaya, the initial isotope values in precipitation falling at Quelccaya, and the isotopic values of the water vapor in the lower troposphere in the western Amazon Basin. They found that Quelccaya's interannual $\delta^{18}O$ variability was most sensitive to lower tropospheric water vapor $\delta^{18}O$ over the western Amazon Basin, which in turn reflected upstream and South American Summer Monsoon (SASM) variability. They found that the SASM influence from ENSO can account for over two thirds of ENSO's influence on isotopic water vapor concentration at Quelccaya. They suggested that this occurs because the SASM is more

active during La Niña and less active during El Niño, resulting in lower water vapor $\delta^{18}O$ values downstream in the lower troposphere over the western Amazon Basin in La Niña events and higher values during El Niño events. El Niño events typically result in a weakening of the SASM because of weaker upper tropospheric easterlies, and the reverse is true in La Niña events.

However, during La Niña events, there is precipitation later in the wet season as well, which helps preserve the low isotopic ratios, because the western Amazon Basin isotopic ratios reach their minimum in the late wet season (Hurley et al., 2019). Additionally, they note that typical northerly low level jets are weaker during La Niña events, perhaps connected to more active cold air incursions from southern South America into the Amazon Basin, which are responsible for much of the precipitation at Quelccaya. Despite the questions that remain and the possible connected explanations for the isotopic signal, Hurley et al. conclude that the isotopic signal at Quelccaya is tied to the hydrologic cycle and large scale circulation patterns associated with ENSO.

1.1.3. Illimani

Studies of Nevado Illimani (16.65S, 67.78W, 6300 m asl) have relied on cores drilled in 1999. Decadal trends were found to be very similar to those at Huascarán, Quelccaya, and Sajama (Knüsel et al., 2005). Knüsel et al. investigated the ENSO signal from 1887-1999 through PCA analysis and found that the strongest ENSO signal was in dust concentration, which was positively correlated with NIÑO3 SSTs (r = 0.36, no p-value given). The highest dust measurements were around 1915, 1942, and 1993, which were all times of persistent El Niño events (Knüsel et al., 2005). They looked at nearby rain-gauge measurements and found that dust values were negatively correlated with precipitation south of Illimani, a region which typically experiences drought conditions during El Niño events through teleconnections with the Pacific although the moisture in this region is of Atlantic origin. They suggested that lower precipitation in this area led to increased dust transport from the region to the ice cap at Illimani. Despite the Atlantic origin of air arriving at Illimani during the wet season, when the majority of precipitation falls, Knüsel et al. found only weak relationships with Atlantic meteorological indices. They found a correlation of 0.29 (no p-value given) between accumulation and the Tropical North Atlantic SST index during the period from 1950–1998.

1.1.4. Sajama

Sajama, Bolivia (18º06’S, 68º53’W, 6542 m asl) is about 9º south of Huascarán, and as the southernmost Andean glacier in the intertropical zone, its summer precipitation comes from convection due to heating of the Altiplano and moist air advection from the Amazon and the La Plata basin (Arnaud & Muller, 2001). Arnaud and Muller compared snowline altitudes with the Southern Oscillation Index (SOI), a measure of sea level pressure differences between Tahiti, French Polynesia and Darwin, Australia, from October to March and found that a high snowline correlates with negative SOI. They found this correlation is more connected with precipitation levels than with temperature, but that both factors are significantly correlated at the 95% level. They connected this pattern with the northward displacement of the Bolivian High during El Niño events. They discussed the high level of snowline rise in 1997-1998 despite a very wet year in 1996-1997, suggesting year to year independence of snowline and showing its potential as an annual climate indicator. Thus, Sajama exhibits a similar trend to that observed on Illimani and Quelccaya, with the warm

phase of ENSO coinciding with warmer temperatures and lower precipitation. Henderson's 1996 study on the 1993 Huascarán core revealed a similar trend with temperature proxies but no strong or consistent link with net accumulation. Additionally, Bradley et al. (2003) found that the $\delta^{18}O$ record from Sajama can be interpreted as reflecting mean SSTs in the central or eastern Pacific.

1.2. El Niño Events

Standardized measurements of ENSO are derived from SST anomalies in different regions throughout the Pacific, including the following which are employed in this project: NIÑO4 (160ºE to 150ºW, 5ºN to 5ºS), NIÑO3.4 (170ºW to 120ºW, 5ºN to 5ºS), NIÑO3 (150ºW to 90ºW, 5ºN to 5ºS), and NIÑO1+2 (from the equator to 10ºS, 90ºW to 80ºW). These regions are shown in Figure 3. NIÑO3.4 is the region most commonly used to define ENSO events, and NOAA typically defines an El Niño or La Niña event respectively as an event in which SSTs in this region reach an anomaly of greater than ±0.5 C for five consecutive three-month running means (NOAA). SOI is a measure of the difference in pressure between Tahiti and Darwin, and it can measure changes in the Walker Circulation.

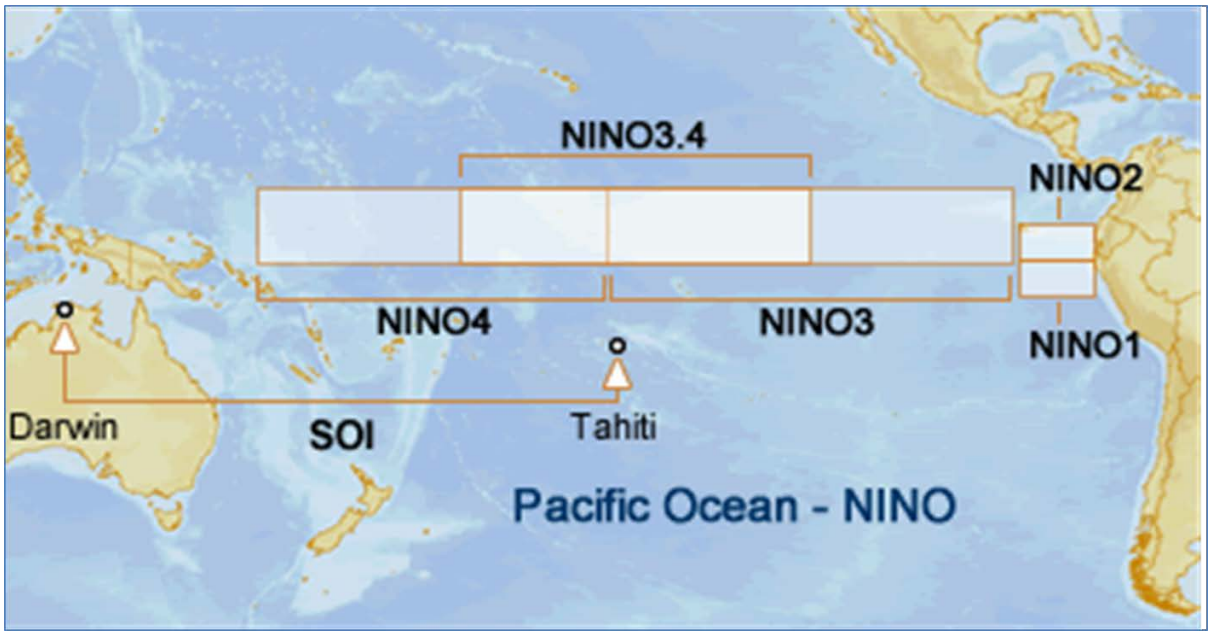

Figure 3: Primary regions in the Pacific Basin that are influenced by El Niño. These regions' SSTs are expressed as standardized monthly indices which, along with other meteorological variables, are examined for their relationship to the annual data from Huascarán using correlation analyses. SOI, the Southern Oscillation Index, is calculated as the sea level pressure differences between Tahiti and Darwin. This figure is modified from http://www.bom.gov.au/climate/enso/indices/about.shtml.

El Niño events are particularly important to the health of South American glaciers as they typically stimulate melting. According to Trenberth et al. (2002), ENSO is responsible for 0.06 ºC of global surface warming occurring between 1950 and 1998. This accounts for 13.6% of the linear trend in surface temperature data from this period. Global warming events peak three months after Niño3.4 SSTs. Oceanic heat excess drives teleconnections because it causes increased evaporation, and therefore, precipitation. Trenberth noted a change in El Niño events in the late 1970s: before 1976, El Niño events began on the west coast of South

America and developed westward, but after 1977 warming began developing from the west. This could be due a phase shift in the phenomenon now known as the Interdecadal Pacific Oscillation (IPO).

It is notable that most of the time period under investigation in this study occurred in what is considered a cold phase of the IPO. While it is contested whether we have entered a warm phase, and if so when that happened, after the 1997-1998 El Niño, there appears to have been a cold phase of the IPO lasting until at least around 2012. The "hiatus" in global temperature increases of the early 2000s was associated with this negative (cold) phase of the IPO (Liu & Xie, 2018). It is difficult for models to simulate the specific period of the hiatus that was observed unless they constrain the end of the negative IPO phase around 2012.

However, two of the three El Niño events under investigation here likely occurred during warm phases of the IPO, or at least share the characteristics of El Niño events from warm phases of the IPO, which tend to be positioned further east in the Pacific than those which occur during the cold phases (Banholzer & Donner, 2014).

1.2.1. 1997-1998 El Niño

In early 1997, the trade winds in the western and central equatorial Pacific weakened and reversed, which led to unusually warm SSTs (McPhaden, 1999). Consequently, the western Pacific warm pool migrated eastward and the eastern Pacific cold tongue failed to develop over the summer. The El Niño developed very rapidly from June to December of 1997, although there was variability in the conditions during its development, including occasional westerly winds particularly in areas over 29ºC due to the Madden-Julian oscillation. The westerly winds stimulated Kelvin waves which forced the thermocline down around 90 meters in the eastern Pacific in late 1997. In the western Pacific, the weakening of the trade winds led to the development of Rossby waves which led the thermocline to become 20-40 meters shallower. The usual east-west gradient of the thermocline therefore disappeared. In the cold tongue region, sea surface temperature anomalies averaged 4ºC and in some areas near the Peruvian coast reached 8-9ºC above normal (McPhaden, 1999).

Thermocline shoaling gradually progressed eastward, but temperatures remained very high in the eastern Pacific until the trade winds abruptly returned to normal strength in May of 1998 (McPhaden, 1999). In the eastern Pacific upwelling resumed and SSTs plunged. At (0°, 125°W), 8ºC of cooling occurred within a month, which is ten times the normal annual cooling rate, and La Niña conditions prevailed by the end of 1998. (McPhaden, 1999).

In terms of biological signal, this El Niño reduced chlorophyll-A in the eastern equatorial Pacific (Gierach et al., 2012). This El Niño event is considered an eastern Pacific (EP) El Niño and was dominated by the dynamics of traditional El Niño events (Paek et al., 2017). The El Niño event was predicted by some models but not others, and few models anticipated the rapidity with which the event would terminate (McPhaden, 1999). Factors modulating this El Niño may include buildup of heat in the western Pacific, the positive phase of the IPO, the recent decades of global heat buildup, and/or the disturbances to the heat in the western Pacific caused by the Madden-Julian Oscillation, which was also in a phase during which strong El Niño events are more likely (McPhaden, 1999).

1.2.2. 2009-2010 El Niño

The 2009-10 El Niño event followed a different pattern than the other two El Niño events in this study. The area with the most extreme temperature anomalies was the central rather than eastern Pacific, and at the time this event broke SST temperature records in the central Pacific (Kim et al., 2011). Because of this center of warming in the central Pacific, the event was considered a Central Pacific (CP), warm pool, or El Niño Modoki event. Such El Niño events tend to correspond less with globally positive temperature anomalies than traditional El Niño events (Banholzer & Donner, 2014). Over its developing and mature phases, this event followed typical CP El Niño patterns in equatorial Pacific SST anomalies (Kim et al., 2011). However, in the Indian Ocean, unusually warm temperatures developed throughout the course of this El Niño event. It could be due to the Indian Ocean warming that easterly wind stress developed over Indonesia and the west Pacific which led to an upwelling Kelvin wave and an unusually fast transition to La Niña conditions the following year (Kim et al., 2011).

In terms of biological signal, this El Niño reduced chlorophyll-A in the central equatorial Pacific (Gierach et al., 2012), in correspondence with its central Pacific highest temperature anomalies. Most El Niño events of the early 21st century have followed this Central Pacific El Niño pattern (Paek et al., 2017).

1.2.3. 2015-2016 El Niño

The 2015-2016 El Niño event set SST records in both the NIÑO3.4 and NIÑO4 regions, though not the NIÑO3 or NIÑO1+2 regions (Stockdale et al., 2017). In 2015, there was warming in April and May, although normally warming occurs primarily in March. Normally, cooling occurs over the summer, and the equatorial Pacific stays cool in the fall and winter due to zonal winds strengthening and upwelling of cooler water at the equator, but in 2015, the Pacific stayed warm all year. Additionally, the Pacific Ocean was warm due to the borderline El Niño conditions present in 2014. This El Niño event technically began when the Oceanic Niño Index (ONI, an index of 3-month averages of NIÑO3.4 SSTs) reached a 0.5ºC positive anomaly in December of 2014, peaked in November of 2015, and lasted 19 months into 2016 (Rupic et al., 2018). The event dissipated in May of 2016 as the eastern Pacific returned to normal or cooler than average temperatures. While ONI was comparable to its 1997-1998 values, in 2015-2016 the tropical Pacific was warmer in the west and cooler in the east. This event was longer than the 1997-1998 El Niño, but while global impacts in the Northern Hemisphere were of similar intensity to those of the 1997-1998 El Niño, impacts on the Southern Hemisphere were slightly less drastic (Rupic et al., 2018).

Globally the Hadley cell strengthened and the position of the jet stream over the North Pacific changed (Stockdale et al., 2017). The new record for the hottest year globally since 1998 was observed, as was the largest one-year increase in Mauna Loa CO_2 values, perhaps because, in addition to the usual increased warming during El Niño events associated with reduced oceanic CO_2 uptake, there were notable forest fires in Indonesia occurring during this event (Lindsey, 2016).

While in many ways this El Niño was comparable in life cycle to the 1997-1998 El Niño–both spread from the South American coast to the International Date Line in boreal springthis El Niño was not a pure EP event (Paek et al., 2017). Maximum sea surface temperature anomalies occurred to the west of those in 1997-1998 and the thermocline

anomalies were less than those of 1997-1998, two characteristics which are more comparable to CP events (Paek et al., 2017). Paek et al. found that CP El Niño onset was related to a negative phase of the North Pacific Oscillation and positive Pacific Meridional Mode SST and wind indices and that, while both of these conditions were present in the beginning of both El Niño events, in 2015-2016, these conditions lasted longer. Therefore, CP dynamics had more influence on the climatology and development of the 2015-2016 El Niño.

1.3. La Niña events

The cold phase of ENSO typically brings effects opposite those of El Niño. Globally averaged temperatures are cooler, and in the Pacific, the thermocline is steeper than average: deeper in the Tropical Warm Pool near Indonesia while the rest of the Pacific is cooler. Typically, the Walker circulation is weaker and stronger easterlies prevail over the Tropics, and below-average SSTs prevail over most of the Pacific while above-average SSTs in the far western Pacific extend northward and southward in a "horseshoe" pattern (L'Heureux, 2008). The climatological pattern is not always the same, however.

1.3.1. La Niña 1998-2000

The 1998-2000 two-year moderate-to-strong event exhibited negative anomalies in the Eastern Pacific but strong Walker circulation in comparison to seven strong La Niña events in the preceding decades (Shabbar & Yu, 2009). Shabbar and Yu argue that unusually warm general tropospheric conditions north of the Tropics on land persisted through 2000 after the 1997-1998 El Niño, in contrast to the typical form of La Niña events. As warm ENSO phases can vary in areas of maximum input and in patterns of teleconnections, so perhaps can the cool events. Shabbar and Yu suggested that North Pacific ocean-atmosphere variability and tropical precipitation anomalies (in this event, the SST anomalies were farther west than their normal position, which led precipitation anomalies to also occur further west than normal) as possible causes of the unusual and El Niño-like discrepancies from typical La Niña patterns during the 1998-2000 event.

1.3.2. La Niña 2007-2008

The 2007-2008 La Niña was in some ways more climatologically typical than the 1998-2000 event; the "horseshoe" SSTs in the Pacific were observed as well as a typical westward retraction of deep tropospheric heating, shown by the retraction of the 200 mb subtropical ridge toward Indonesia (L'Heureux, 2008). This was a strong La Niña with an ONI value of -1.5 during DJF. L'Heureux notes a very active Madden-Julian Oscillation from mid-November of 2007 to February of 2008, with these eastward propagating disturbances making their way around the globe three times in the season and shifting a convective signal eastward over the tropical Indian and western Pacific Oceans.

1.3.3. La Niña 2010-2012

After the 2009-2010 El Niño, the Indian basin warming led to strong equatorial easterlies that helped push the climate system into a La Niña phase (Feng et al., 2013). The event peaked in October of 2010 and included moderate-to-strong conditions throughout late 2010 to the spring of 2011 (Zhang et al., 2013). Easterly wind stress anomalies in the equatorial western Pacific were unusually high toward the end of 2010, and there were positive sea level anomalies in the western tropical Pacific (2010). Neutral conditions prevailed in April-June of 2011, but by fall of 2011, weak-to-moderate La Niña conditions resumed (Zhang et al., 2013). In mid-2011 there were two conflicting factors that made

prediction of the next months' SSTs difficult. These were the buildup of heat content in the western Pacific whose propagation would lead to rising temperatures in the eastern Pacific, and negative anomalies of subsurface water entrained into the mixed later in the central equatorial region exerting a cooling influence. The latter prevailed, and weak La Niña conditions continued through early 2012.

1.4. Climatology of Huascarán

The seasonal shift of the ITCZ is integral to the climate of Huascarán, which, being located between 0-30ºS would experience SE winds under ideal climatological conditions. According to Garreaud et al. (2009), except during intense El Niño events, the ITCZ in the Pacific Ocean lies north of 5ºN throughout most of the year whereas throughout South America it is more seasonally variable. In austral winter, continental rainfall is located north of the equator, near the oceanic ITCZ. Huascarán lies squarely within the zone receiving predominantly SE winds but is also affected by the Bolivian High, an upper-level high-pressure cell caused by latent heat released by cumulus convection over the Amazon Basin (Garreaud et al., 2009). Additionally, the region is indirectly affected by climate patterns in the Atlantic. Garreaud et al. note that droughts in the Amazon and northeast Brazil seem to be linked to warmer temperatures in the tropical northern Atlantic, which is notable because the Atlantic is the source of moisture throughout almost all of tropical South America. Areas south of Huascarán often experience drought-like conditions during the ENSO cold phase while areas to the north often experience increased precipitation due to a southward ITCZ shift which induces dry conditions in the Altiplano (Sulca et al., 2017).

In a typical year, by the end of October, a broad area of precipitation shifts from the southern half of the Amazon to northern Argentina, a phenomenon sometimes characterized as monsoon-like (Garreaud et al., 2009). The South American Summer Monsoon (SASM) drives seasonal variation because precipitation comes from the Amazon, and despite the seasonality of precipitation, there are no large differences in temperature throughout the year in the Cordillera Blanca where temperature variations are primarily driven by altitude (All et al., 2017). However, Davis et al. (1995) found that based on Automated Weather Station (AWS) data, the seasonal temperature difference on Hualcán (a mountain near Huascarán) was ~9º, significantly greater than that on Quelccaya (~2º), indicating that around Huascarán there may be significant seasonal differences in temperature as well.

After March, there is little snow accumulation at Huascarán. On an annual basis at Huascarán, Davis et al. (1995) found that increased microparticle and nitrate concentrations occurred in the dry season due to higher radiation and lower snow accumulation. In this season there are strong north-easterly winds at the 500 mb level.

2. Methodology

2.1. Determination of annual values

2.1.1. Retrieval of cores and chemical analyses

Two ice cores were retrieved in 2019 from the ice field in the col of Huascarán Mountain by the Ice Core Paleoclimatology Research Group (ICPRG) at the Byrd Polar and Climate Research Center (BPCRC). The ice cores were brought back to the freezers in Columbus, Ohio and analyzed for concentrations of fluoride (F^-), chloride (Cl^-), sulfate (SO_4^{2-}), nitrate (NO_3^-), sodium (Na^+), ammonium (NH_4^+), potassium (K^+), magnesium (Mg^{2+}), calcium (Ca^{2+}), MSA (methane sulfonic acid, $CH_3SO_3^-$),$\delta^{18}O$ and δD. Ionic species were measured by ion chromatography using a Dionex ICS-5000 and the dust concentrations were measured using a Beckman-Coulter Multisizer 4, both in a Class 100 Clean Room. The isotopic measurements were made in the isotope laboratory with a PICARRO cavity ring-down spectroscopy analyzer.

2.1.2. Determination of dry season peaks

The annual values for each core constituent were determined by identifying seasonal peaks in both $\delta^{18}O$ and nitrate concentrations and by comparison with similar peaks in the 1993 core also drilled on the Huascarán col. These peaks occur around July in the austral winter which is the dry season (Fig. 2). The peak in $\delta^{18}O$ enrichment and the peak in nitrate concentrations occur at this time allowing determination of the successive thermal years (dry season to dry season or July to July). The thermal year, which lasts from dry season to dry season and is centered around one wet season, is marked as the calendar year which begins in its middle. That is, the period from July of 2018 to July of 2019 is referred to as the 2019 thermal year. Annual values of all parameters other than net accumulation were computed by averaging the values of all the samples comprising the section of core containing each thermal year as shown in Figure 2.

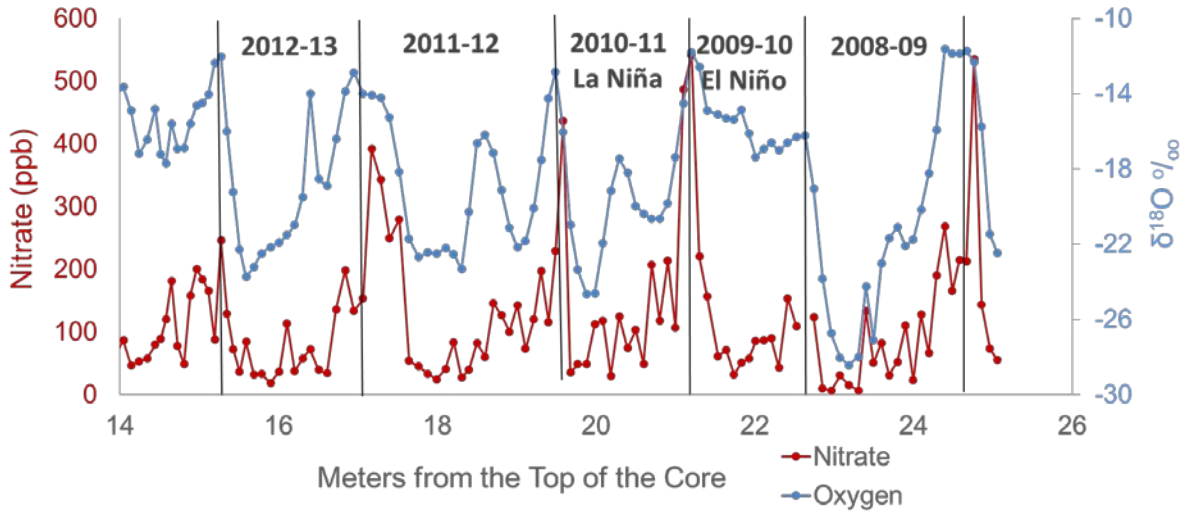

Figure 2: The nitrate and $\delta^{18}O$ records from 2008-2013 (15-25 m) reveal the dry season peaks used to identify each austral winter, thereby providing a timescale for the core.

This method of dating the core places the primary emphasis on the wet season, because only the wet seasons are clearly separated from each other. In other words, depending on the exact delineation of the years, a sample from the dry season of one year may be included in the thermal year preceding or following this dry season. Thus, the clearest signals will occur in the key wet season indicators, net accumulation and $\delta^{18}O$. Additionally, the largest precipitation anomalies linked with ENSO in South America occur during the austral summer (the wet season), and therefore this method of delineating annual values will be particularly effective at capturing ENSO variability in precipitation.

2.1.3. Net accumulation

Net accumulation in meters of ice equivalent (m.i.e.) accumulation was determined by first finding the length of the core in each thermal year. Using the density measurements taken throughout the ice core and a polynomial was fit to the data plotted as depth versus density allows the density to be calculated for any depth in the core. This calculated density was in meters of water equivalent (m.w.e.) and was used to convert each core sample into its respective water equivalent length. The water equivalent length was then adjusted to the ice equivalent length assuming an ice density of 920 kg m^{-3}.

Now that the length of year was known in ice equivalent, the annual layers must be adjusted for thinning with depth. The equation used for thinning was $a = l'(1-z'/h')^{-(p+1)}$ where a = ice equivalent precipitation, l' = density-normalized layer thickness, Z'=center depth of layer in question, H' = the thickness of glacier, and P is a thinning parameter (Henderson, 1996). The value for the thinning parameter used here, 1.253, was estimated by Henderson who worked with the 1993 core from the same location. The thinning-normalized accumulation values calculated are the net accumulation values checked for correlation with various climatological parameters throughout this study.

Due to uncertainties in the process used to account for thinning, in addition to using the thinning-normalized data to examine correlations between SST indices and the net accumulation, the net accumulation values which were not thinning-normalized were analyzed as well. For this measurement, the average value of the years preceding and following the ENSO event was compared with the accumulation value during that specific event. Through this process comparisons were made between the net accumulation of the years in question and the surrounding years at a similar depth in the core.

2.2. Normality testing

Annual data for each chemical or physical record in the core were tested for normality using the Shapiro test of normality. Five records failed the assumption of normality: F^-, MSA, Cl^-, Na^+, and K^+. These chemical records were therefore excluded from the statistical analysis performed on the rest of the data.

2.3. Statistical tests performed

The top 44 meters of the core were used in this study and represent the period from 1994 to 2019. This time period contains three major El Niño events: 1997-8, 2009-10, and 2015-6 and three major La Niña events spanning four wet seasons: 1998-1999, 1999-2000, 2007-2008, and 2010-2011. For statistical analysis, these three El Niño years were combined into a group which was then compared to the group containing all other years (including La Niña years) using student's t-tests to examine the data for differences in all markers.

Similarly, wet seasons occurring during La Niña events were combined into a group and compared to a group containing all other years (including El Niño years) for t-tests as well. To test the significance of these t-tests, analysis of variance (ANOVA) was performed with El Niño years, La Niña years, and the baseline (a group including all data from 1994-2019 excluding the three El Niño years and four La Niña years) as the three groups under comparison.

Additionally, correlation coefficients were computed between all yearly values and all SST indices. Corresponding SST values were determined by averaging the Dec-Feb values from each of NOAA's various equatorial Pacific temperature and pressure indices (NIÑO4, NIÑO3.4, NIÑO3, NIÑO1+2, and SOI,) as well as indices recording Atlantic SSTs (AMO, TSA, and TNA). The AMO, or the Atlantic Multidecadal Oscillation, measures SSTs in the Atlantic from 0-80ºN. The Tropical South Atlantic Index (TSA) measures SSTs from 30°W-10°E, 20°S-0°, while the Tropical North Atlantic Index (TNA) measures SSTs from 55°W-15°W, 5°N-25°N.

The wet season period from December to February was used for these climate parameters because it is when the majority of precipitation is deposited on the Huascarán. While previous studies found stronger signals by using smoothed data, this analysis was not performed here as the short length of record (1994 – 2019) did not allow for significant smoothing. The variety of SST measures were used to determine the region in the ocean whose SSTs had the strongest relationship to the proxy records.

NOAA Reanalysis modeled regional meteorological data including upper tropospheric temperatures, outgoing longwave radiation (OLR), and geopotential height (GPH) at the 500 mb level (available at https://psl.noaa.gov/cgi-bin/data/timeseries/timeseries1.pl) were tested by correlation analysis for statistically significant relationships with all data records from Huascarán. The statistical relationships between NIÑO4 SSTs and all Reanalysis metrics (OLR, 500 mb GPH, and temperatures at 500, 400, 300, 250, 200, and 150 mb) were calculated.

2.4. Back trajectories

Atmospheric back trajectory analysis was performed using NOAA's Hybrid Single-Particle Lagrangian Integrated Trajectory (HYSPLIT) software (Rolph et al., 2017, Stein et al., 2015). Weeklong trajectories were plotted using Reanalysis modeled data for the wet seasons of the three El Niño events, three of the wet seasons occurring during La Niña events (1998-1999, 2007-2008, and 2010-2010), as well as three years which were selected for their neutral Pacific SSTs during the wet season (2001-2002, 2003-2004, and 2013-2014). Trajectories were produced every 6 hours for the period from December 7th-February 28th of these years, and the trajectories were plotted as frequency images.

Seventy-two hour trajectories from the same times were used for cluster analysis. HYSPLIT suggests several numbers of clusters which present less internal variability than other numbers of clusters based on the total spatial variance between the clustered trajectories. Plots of the total spatial variance compared to the number of clusters is shown in the Appendix. The number of clusters was determined by the number with the least spatial variance that was closest to five. Clusters were used to provide more quantitative evidence for the difference between El Niño, La Niña, and neutral events, while frequency plots were used for visual comparison. Clusters were derived from the same 6-hour intervals of

trajectories throughout the wet season that were used for the frequency analysis, but only the first 72 hours of these trajectories were used.

Plots of the dry seasons which are shown in the Appendix were produced for several years for examples of El Niño, La Niña, and neutral events. Two two-year cycles were analyzed using monthly frequency plots, during the La Niña event from 1998-2000 and the El Niño from 2014-2016. These monthly plots were used to examine the difference between the development of El Niño and La Niña events.

2.5. Observed meteorological data

Observed meteorological data from this region are often inconsistent and biased toward lower altitudes, although consistently observed data would be invaluable to this study because of the possible errors associated with use of satellite data. However, Villavicencio Guillén (2019) compared monthly precipitation data from several sites throughout the Ancash region of Peru in which Huascarán is located to satellite data from TRMM and GPM, and temperature data at these sites to satellite data from MERRA-2 for a period from 2012-2018. He found that there was high correlation between observed and satellite data for this period. In the region of Huascarán (Santa), he found a correlation of R^2=0.816 with GMP satellite data and of R^2=0.497 with TRMM satellite data. Temperature records are more important for this study, however, because it used satellite temperature data at many atmospheric levels. For temperature, the strength of the correlation varied by month and depended partially on cloudiness and fog. Correlations between observed and satellite temperature records ranged from R^2=0.725 in August to R^2=0.952 in February. Based on these strong correlations, particularly in the wet season on which the ice core record is focused, it was assumed that the satellite data provided a sufficient record of actual temperatures. Because of the general reliability of the satellite data and the paucity of observed records in this region, this study has used primarily satellite data as its most direct source of temperature data.

3. Results and discussion

3.1. Isotopic signal

3.1.1. $\delta^{18}O$ and δD

The strongest correlations between any Huascarán record and the SST indices were for the isotopic ratios and the NIÑO4 SST averages for December through February (wet season), which is consistent with previous results by Henderson (1996) who only investigated correlations with NIÑO3.4 SSTs. Correlation coefficients for $\delta^{18}O$ and δD with NIÑO4 were 0.682 and 0.672 ($p<0.001$), respectively. The correlation between NIÑO4 SSTs and $\delta^{18}O$ are shown in Figure 4. Given their close relationship, the same correlations with δD are very similar (Table 2), no plot is provided between δD and NIÑO4 SSTs, as it is virtually identical to Figure 4. Relationships between $\delta^{18}O$ and the various Atlantic and Pacific SST indices, as well as upper tropospheric temperatures, the geopotential height (GPH) of the 500 mb level, and outgoing longwave radiation (OLR) at Huascarán are shown in Table 1 and the results for the same variables compared to δD are shown in Table 2.

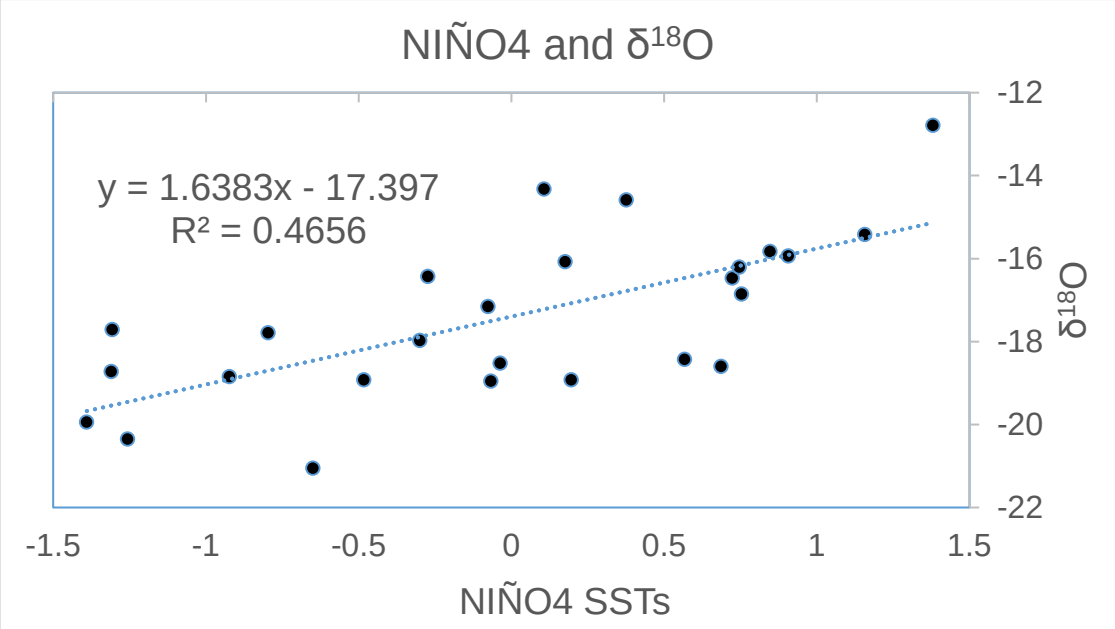

Figure 4: Correlation between NIÑO4 SSTs and $\delta^{18}O$

The strongest correlations for $\delta^{18}O$ and δD are with NIÑO4 although NIÑO3.4, SOI, and NIÑO3 are also significantly correlated at the $p<0.05$ level. The farther west the Pacific SST index, the stronger the correlation with $\delta^{18}O$. There are also high correlations with OLR ($r=0.689$, $p<0.001$) and with upper tropospheric temperatures, particularly at the 200 and 500 mb levels ($r=0.593$ and $r=0.602$, respectively, $p=0.001$).

These data indicate warmer temperatures during El Niño events, although this result may be compounded by precipitation effects in these years, particularly the reduced depletion of ^{18}O and ^{2}H through decreased strength of the SASM as discussed earlier (Hurley et al., 2019). To the south on Sajama, Arnaud and Muller (2001) found net accumulation to be a stronger driver of the upward shift in the glacier's snowline than temperature during El Niño events. However, the relationship between $\delta^{18}O$ and NIÑO4 is much stronger on Huascarán than that for net accumulation and NIÑO4. Although the precipitation "amount effect" seems

to have a strong impact on other Andean ice fields, the correlations with Pacific SSTs are higher for $\delta^{18}O$ than net accumulation at Huascarán, suggesting that the temperature effect is stronger than the precipitation amount effect. Net accumulation is discussed in greater detail later in the paper.

Table 1: Correlations between $\delta^{18}O$ and Pacific and Atlantic SST indices, a Pacific surface pressure index (SOI), and modeled climatological data at Huascarán.

climate measurement	$\delta^{18}O$ r value	p-value
NIÑO1+2	0.344	0.085
NIÑO3	0.577	0.002
NIÑO3.4	0.661	<0.001
NIÑO4	0.682	<0.001
SOI	-0.626	<0.001
AMO	0.253	0.212
TSA	0.203	0.321
TNA	0.236	0.257
500 mb temps	0.620	<0.001
400 mb temps	0.465	0.017
300 mb temps	0.410	0.038
250 mb temps	0.482	0.013
200 mb temps	0.627	<0.001
150 mb temps	0.579	0.002
GPH 500 mb	0.546	0.004
OLR	0.693	<0.001

Table 2: correlations between δD and Pacific and Atlantic SST indices, a Pacific surface pressure index (SOI), and modeled climatological data at Huascarán.

climate measurement	δD r value	p-value
NIÑO1+2	0.319	0.112
NIÑO3	0.552	0.003
NIÑO3.4	0.642	<0.001
NIÑO4	0.672	<0.001
SOI	-0.600	0.001
AMO	0.243	0.232
TSA	0.203	0.320
TNA	0.278	0.168
500 mb temps	0.602	0.001
400 mb temps	0.442	0.024
300 mb temps	0.386	0.051
250 mb temps	0.457	0.019
200 mb temps	0.593	0.001
150 mb temps	0.540	0.004
GPH 500 mb	0.525	0.006
OLR	0.689	<0.001

3.1.2. Deuterium excess

Deuterium excess (d) measures the difference between the $\delta^{18}O$ and δD measurements as compared with global averages. It is defined through the equation $d = \delta D - 8\ \delta^{18}O$ (Dansgaard, 1964). Deuterium excess is the only tracer exhibiting statistically significant higher correlations with an index other than NIÑO4, as it correlates most strongly with NIÑO1+2 SSTs. This relationship is consistent with this proxy's use as a tracer of water vapor origin as there is very little precipitation of direct origin from the central Pacific. Trajectory analysis reveals that normally there is some input from the western Pacific and that this increases during El Niño events as is discussed later. Precipitation reaching the Andes from the Amazon is highly recycled, with recycling rates on the order of 70-80% in this region (Rocha et al., 2018). Recycled water tends to have higher deuterium excess due to differences in fractionation with molecular weight according to the Rayleigh approach. Therefore, the significant negative correlation ($r = -0.4695$, $p = 0.016$) with NIÑO1+2 values for the wet season could reflect increased input from the western Pacific during El Niño years and the absence of this during La Niña phases. It is notable that the correlation with NIÑO1+2 is stronger ($r = -0.536$, $p < 0.005$) if the entire thermal year (July-June) is employed rather than just the wet season value. Table 3 shows relationships between d-excess and the various Atlantic and Pacific SST indices as well as Pacific sea level pressure, upper tropospheric temperatures, the GPH of the 500 mb level, and OLR at Huascarán.

Table 3: correlations between d-excess and Pacific and Atlantic SST indices, a Pacific surface pressure index (SOI), and modeled climatological data at Huascarán.

climate measurement	deuterium excess r value	p-value
NIÑO1+2	-0.469	0.016
NIÑO3	-0.450	0.021
NIÑO3.4	-0.406	0.039
NIÑO4	-0.278	0.169
SOI	0.373	0.060
AMO	-0.136	0.509
TSA	-0.272	0.179
TNA	-0.233	0.252
500 mb temps	-0.374	0.060
400 mb temps	-0.404	0.041
300 mb temps	-0.417	0.034
250 mb temps	-0.439	0.025
200 mb temps	-0.377	0.058
150 mb temps	-0.243	0.232
GPH 500 mb	-0.352	0.078
OLR	-0.176	0.391

Table 3 shows that wet season d-excess values at Huascarán correlate significantly with NIÑO1+2 and NIÑO3 SSTs as well as with SOI and upper air temperatures between 500 and 250 mb. The strongest correlation is between deuterium excess and NIÑO1+2 SSTs (Fig. 5). In Figure 6, the 1997-1998 El Niño event is excluded as this one data point heavily influenced the correlation due to its anomalously high SST value in the NIÑO1+2 region. If this thermal year is excluded the correlation becomes insignificant ($r = -0.091$, $p=0.667$) and

the model's slope becomes flatter. Due to the short time-frame of this study, this one year has a large effect. Not only does the correlation with NIÑO1+2 disappear without the 1997-1998 event; when the dataset excluding 1997-1998 was checked for correlation with all climate parameters in Table 3, there were no significant correlations with any parameters. Perhaps future studies examining deeper parts of the core will be able to identify whether a low deuterium excess value is a common occurrence in EP El Niño events, of which the 1997-1998 El Niño event was the only example in this study.

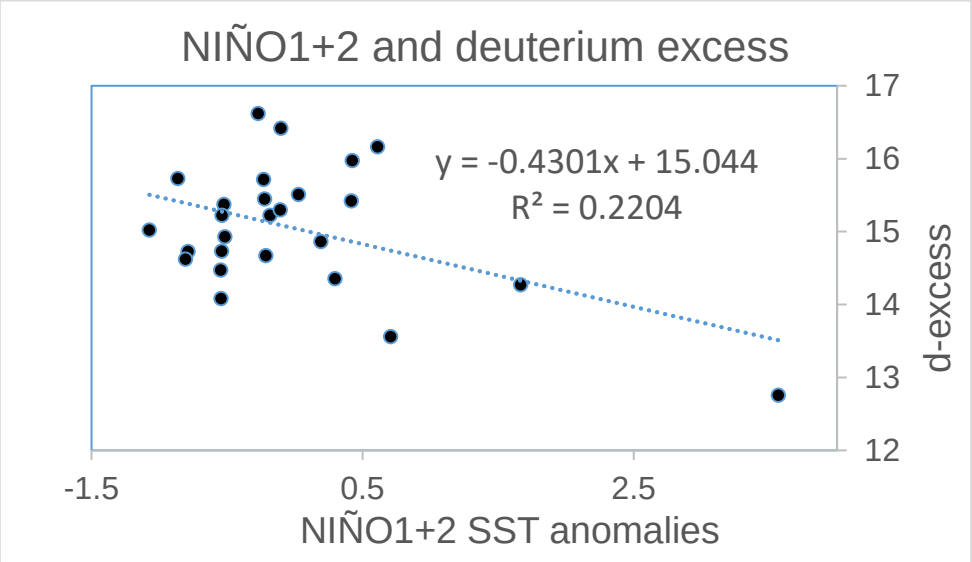

Figure 5: Deuterium excess compared to NIÑO1+2 SSTs from 1994-2019.

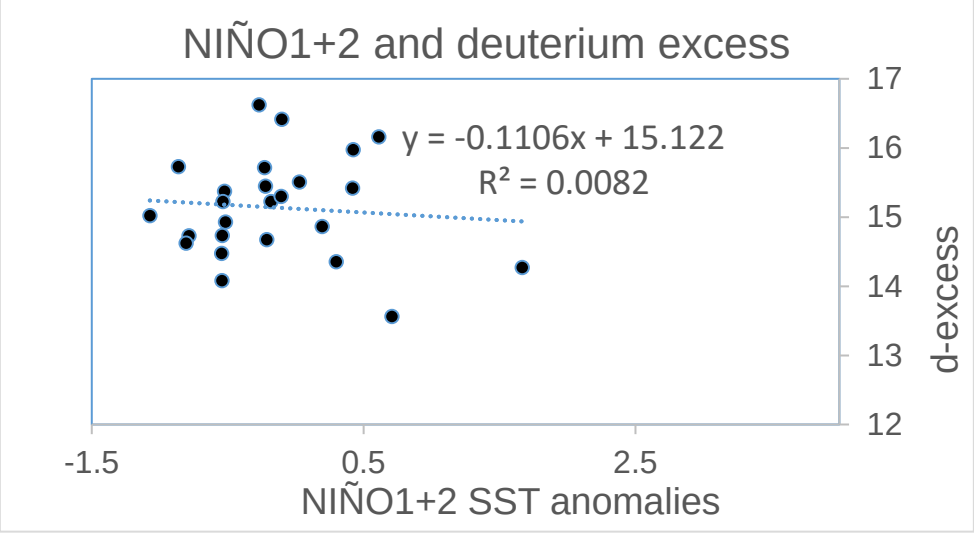

Figure 6: Deuterium excess compared to NIÑO1+2 SSTs from 1994-2019 but excluding the 1997-1998 Eastern Pacific El Niño event.

3.2. Net accumulation

A negative correlation ($r = -0.451$, $p = 0.021$) exists between net accumulation and NIÑO4 (Fig. 7). This SST index had the strongest correlation with net accumulation although correlations with NIÑO3.4, NIÑO3, and TSA were also significant at the $p < 0.05$ level (Table 4). As with the isotopic signal, the relationship between net accumulation and Pacific SST indices increased with distance to the west in the Pacific. Table 4 demonstrates a

negative correlation with tropical South Atlantic SSTs in addition to the link with NIÑO4. This negative correlation between Pacific SSTs and accumulation is consistent with observations on Quelccaya as well as on Illimani (da Rocha Ribeira et al., 2018) for the 1960–1999 period. Henderson et al. (1999) found a connection with the upper air wind vectors over the tropical south Atlantic, but they did not find a link with SSTs in the Atlantic. They suggested that during El Niño events, the Atlantic coast of South America responds to Pacific SST anomalies through an atmospheric bridge, the weakening of the trade winds, which results in wind stress anomalies. Additionally, a negative correlation was found between upper tropospheric temperatures at 500 mb, 200 mb, and 150 mb at Huascarán and the net accumulation.

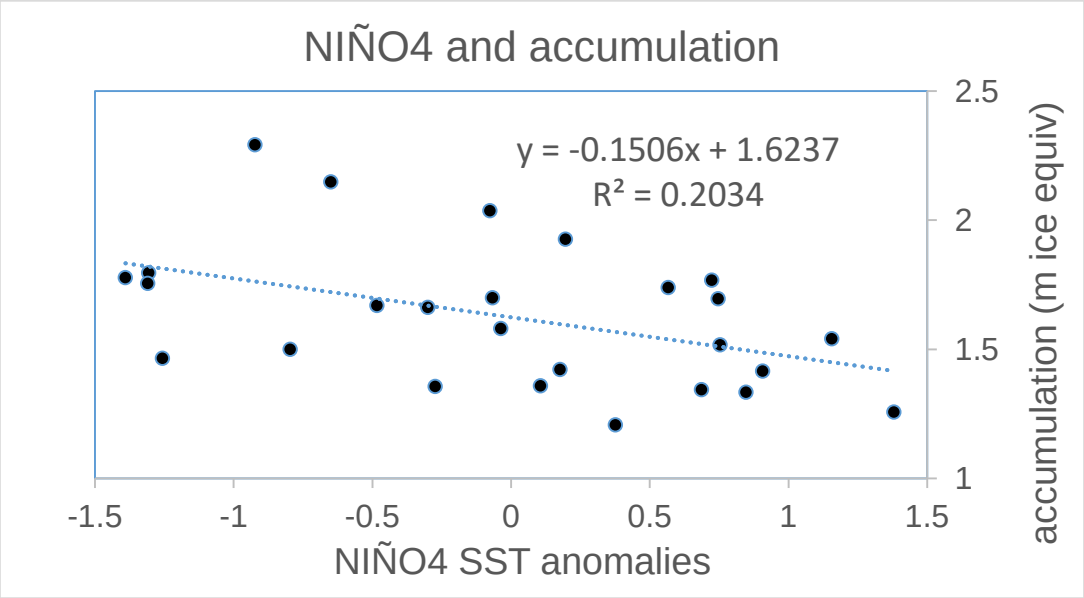

Figure 7: NIÑO4 SSTs and accumulation.

Table 4: correlations between net accumulation and Pacific and Atlantic SST indices, a Pacific surface pressure index (SOI), and modeled climatological data at Huascarán.

climate measurement	Net accumulation r value	p-value
NIÑO1+2	-0.296	0.142
NIÑO3	-0.397	0.045
NIÑO3.4	-0.433	0.027
NIÑO4	-0.451	0.021
SOI	0.385	0.052
AMO	-0.073	0.724
TSA	-0.419	0.033
TNA	-0.340	0.096
500 mb temps	-0.379	0.056
400 mb temps	-0.312	0.121
300 mb temps	-0.266	0.189
250 mb temps	-0.328	0.102
200 mb temps	-0.421	0.032
150 mb temps	-0.443	0.024
GPH 500 mb	-0.376	0.058
OLR	-0.352	0.078

Henderson (1996) found no significant relationship between accumulation on Huascarán and accumulation on Quelccaya, nor between accumulation on Huascarán and ENSO. He found a reduction of 10% or less in layer thicknesses associated with El Niño events. For the three El Niño events in this study, the average accumulation reduction compared with the year immediately before and the year immediately after was 16.5%. For the 1997-1998 and 2009-2010 events, the reduction was 13% in each event, slightly stronger than what Henderson observed, though still not as large as the ~20% reduction on the QIC during El Niño events. However, in 2015-2016, the accumulation reduction compared with the years immediately before and after was 22%. This is consistent with the observed record that the drought extended farther north than is usual in the 2015-16 El Niño. Henderson suggested that the relationship between QIC net accumulation and ENSO could be related to the northern reaches of the upper level westerlies, which do not affect Huascarán. Whether the drought's northern extension in 2015-16 suggests anything about the future of the upper-level westerlies during El Niño events cannot be ascertained at this time, because there is only one such observation in this study.

It is also notable that the majority of the study occurred during a cold phase of the IPO, which is connected to more central Pacific El Niño events as is discussed in the introduction. Sulca et al. (2017) found that central Pacific warming was associated with dry anomalies in the tropical Andes through N-S displacement of the South Pacific Convergence Zone (SPCZ). Therefore, while it is possible that this negative accumulation trend is part of a broader trend in the region of ENSO-associated drought in the Andes due to climate change, it is also possible that it is associated with interdecadal Pacific variability which would not have affected Henderson's longer 1996 study.

Over the course of the four wet seasons in La Niña events, on average there was a 6% increase in accumulation as compared to the years immediately before and after the events. While the 1998-2000 event included increased precipitation (between the two wet seasons there was a 25% increase in precipitation over the average values from 1997-8 and 2000-2001), the 2010-11 La Niña actually included decrease in accumulation as compared to the years surrounding it (19% decrease), and the 2007-8 La Niña was virtually the same as the average of the years surrounding it (5% decrease in accumulation). It is notable that the event with a strong increase in precipitation was a La Niña event with a center of temperature and precipitation anomalies farther west than normal (Shabbar & Yu, 2009).

The relative contribution between the El Niño and La Niña events the ENSO signal in accumulation was explored, because so many of the La Niña events in this timeframe immediately follow El Niño events and therefore the differences between the consecutive years may fail to show which is causing the signal. ANOVA testing failed to reject the null hypothesis that there are any significant difference between the El Niño and La Niña and the baseline (the 18 thermal years not in the El Niño or La Niña groups) accumulation group means ($p=0.24$). However, p-values between the groups El Niño and La Niña and between El Niño and baseline are 0.25 and 0.27, respectively, whereas the p-value between La Niña and the baseline is over 0.9. Therefore, we can fairly well exclude the possibility that this dataset indicates a relationship between La Niña and accumulation, while a longer dataset might contain a relationship between El Niño and the baseline or between El Niño and La Niña.

3.3. Dust

There are also positive relationships (r>0.3) between NIÑO4 SST and the concentration of all sizes of dust greater than 3.14 μm diameter (p<0.1). This relationship is only statistically significant (p<0.05), however, for dust between 5.04 and 8 μm. The relationships between total dust concentrations (diameters 0.63-16 μm) and the various Atlantic and Pacific SST indices, Pacific sea level pressure differences (SOI), as well as upper tropospheric temperatures, the GPH of the 500 mb level, and OLR at Huascarán are shown in Table 5. Total dust is never significantly correlated with Pacific SST indices. Dust does, however, exhibit significant positive relationships with upper tropospheric temperatures from 500-250 mb and with GPH at the 500 mb level

It is also notable that there were statistically significant relationships between the Atlantic Multidecadal Oscillation and the dust values (diameters > 1 μm), MSA, and K^+, although MSA and K^+ were excluded from the study as they failed the normality test. Additionally, it should be noted that while typically correlations were calculated with averages of climate parameters from Dec-Feb of the thermal year in question, for the AMO values from Nov-Jan were used because they correlated more strongly with dust. The dust may be of North African origin, although its origin has yet to be chemically determined but this may be investigated in the future. However, if it is of Saharan origin, that would provide a reason for the apparent Atlantic modulation. Even if the dust is of local or Amazonian origin, it may be affected by the strength of the tropical easterlies, which may, in turn, be affected by Atlantic SSTs. Correlation between the AMO and total dust concentrations (diameters 0.63-16 μm) is shown in Figure 8.There is a strong positive correlation between total dust and K^+ ($r = 0.501$, $p=0.009$) because K^+ is a known chemical constituent of the dust, suggesting that the relationship between K^+ and the AMO and between dust and the AMO may be modulated by the same factor.

Table 5: correlations between dust concentration and Pacific and Atlantic SST indices, a Pacific surface pressure index (SOI), and modeled climatological data at Huascarán.

climate measurement	dust r value	p-value
NIÑO1+2	0.189	0.356
NIÑO3	0.237	0.243
NIÑO3.4	0.227	0.265
NIÑO4	0.202	0.322
SOI	-0.168	0.413
AMO	0.574	0.002
TSA	0.247	0.223
TNA	0.322	0.109
500 mb temps	0.433	0.027
400 mb temps	0.525	0.006
300 mb temps	0.589	0.006
250 mb temps	0.544	0.004
200 mb temps	0.201	0.324
150 mb temps	-0.056	0.787
GPH 500 mb	0.525	0.006
OLR	-0.073	0.723

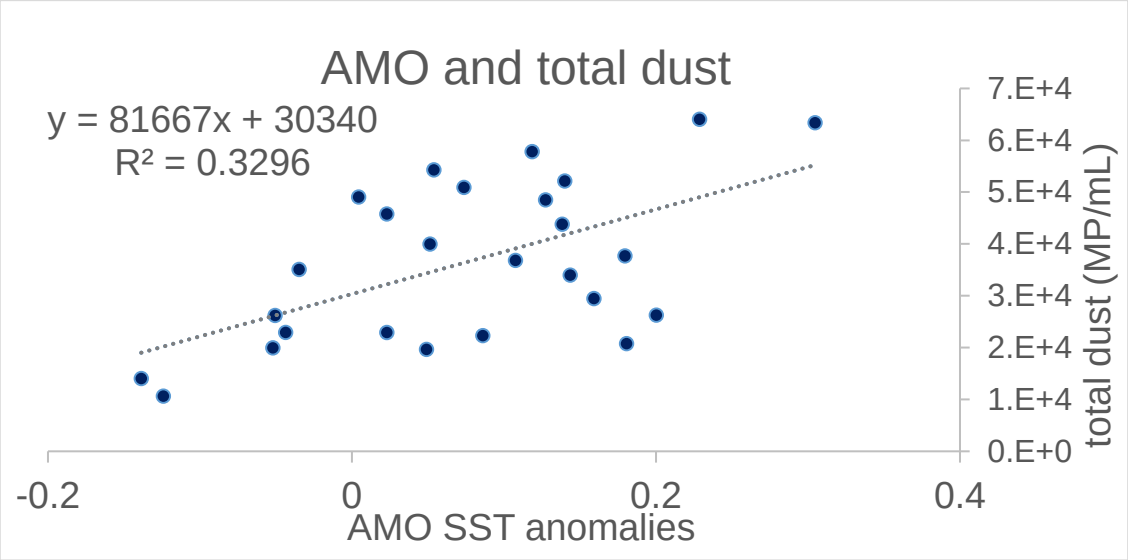

Figure 8: Atlantic Multidecadal Oscillation and total dust

3.4. Sulfate

Sulfate values were significantly (p=0.033) lower during El Niño years as compared to the rest of the dataset. When ANOVA was performed to separate both El Niño and La Niña years from the neutral years, this relationship with sulfate disappeared. Sulfate values were much lower in 2015 than 2009 and 1997, which are comparable to each other but about one standard deviation below the average value of the dataset.

Sulfate may be lower in El Niño years due to the decreased biological productivity of the Peruvian coast after the cessation of upwelling, although the signal is probably at least partially anthropogenic (which may be related to the smaller number of fishing ships in these years). This signal is unlikely to be related to forest fires, since those are more common in El Niño years in the Amazon and would therefore lead to the opposite signal. But the source of the signal—anthropogenic vs. natural—should be evident deeper in the core. If the signal is present deep in the core, it is likely of natural origin.

3.5. Air mass origin during El Niño, La Niña, and neutral years

HYSPLIT back-trajectory analysis reveals differences in the frequency of the origin of air masses bringing precipitation to Huascarán under El Niño, La Niña, and neutral conditions. Figure 9 shows a key for the HYSPLIT frequency trajectories. The wet season from Dec 2001-Feb 2002 characterizes a neutral year (Fig. 10) while the wet season from Dec 1998-Feb 1999 characterizes a La Niña year (Fig. 11). These examples demonstrate the typical amount of Pacific input received on Huascarán during these ENSO events, with modest Pacific input received under neutral conditions and very little during La Niña events. Plots of air mass trajectories for other La Niña and neutral years are included in the Appendix. Figures 12-15 show the air mass origin during the 1997-1998, 2009-2010, and 2015-16 El Niño events, respectively.

The seven day HYSPLIT trajectories during the wet season in the 1997-1998, 2009-2010, and 2015-2016 El Niño events, respectively, reveal the increased Pacific input at Huascarán, particularly in the 2015-2016 El Niño event. Except for 2007-2008, in the La

Niña years, the seven-day trajectories come from much closer to the source than in other years, and in the El Niño years, there is a much larger region of possible trajectory endpoints. Most of this variation comes from the amount of Pacific input there is into the circulation at Huascarán during El Niño events. The neutral years fall between theses extremes. This result would support the conclusion that the most Pacific input to the circulation at Huascarán occurs in El Niño years, the second most in neutral years, and the least in La Niña years. The 2007-2008 La Niña in some ways looks more like a neutral year than a La Niña year. L'Heureux (2008) notes that there was a very active Madden-Julian Oscillation from mid-November of 2007 to February of 2008, with these eastward propagating disturbances making their way around the globe three times in the season and shifting a convective signal eastward over the tropical Indian and western Pacific oceans.

The dry seasons (here meaning May-August so that they fall primarily in one thermal year, even though the dry season peaks in JJA and lasts until around October) include air from further to the east than during the wet seasons (December-February). These are shown in the Appendix and reveal that, in this season too, there is more westerly circulation when there are higher SST anomalies in the central/eastern Pacific. During the very neutral conditions in 2002, there was some circulation from Australia. In the El Niño conditions of 2015, there was considerable Pacific input with much from up to 150ºW, some of which reached Australia. 1998's disintegrating El Niño conditions were similar, but without the few trajectories originating from Australia. However, in the La Niña conditions of both 2010-2011 and 1999-2000 there was almost no circulation from west of 120ºW.

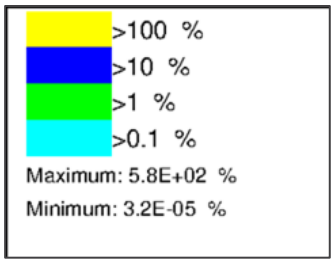

Figure 9: key to HYSPLIT frequency trajectories

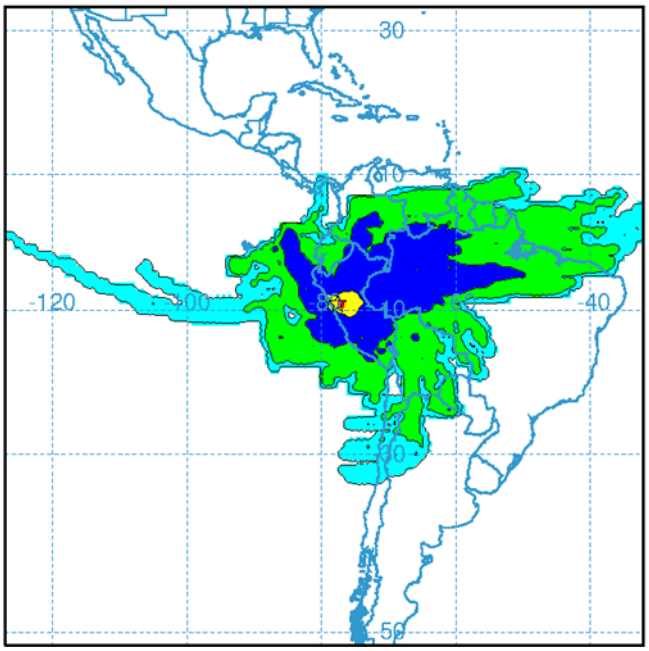

Figure 10: Seven day back trajectories during the wet season (2001-2002) under neutral ENSO conditions

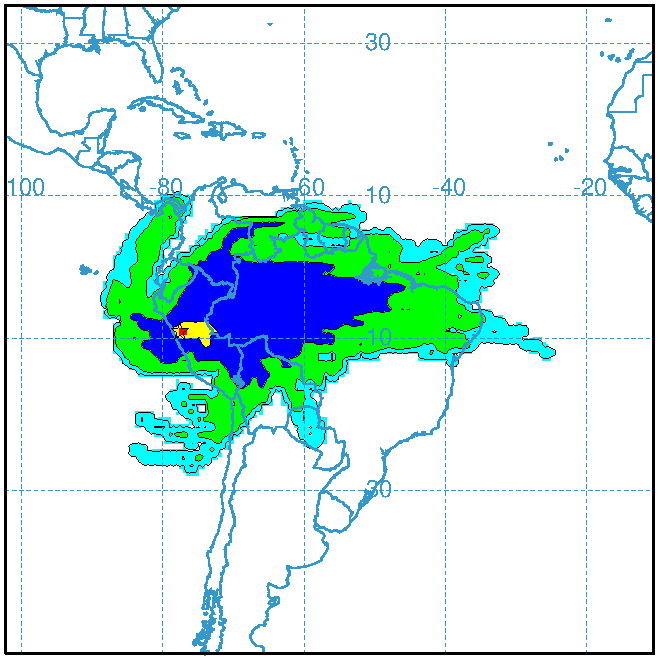

Figure 11: Seven-day back trajectories during the wet season (1998-1999) under La Niña conditions

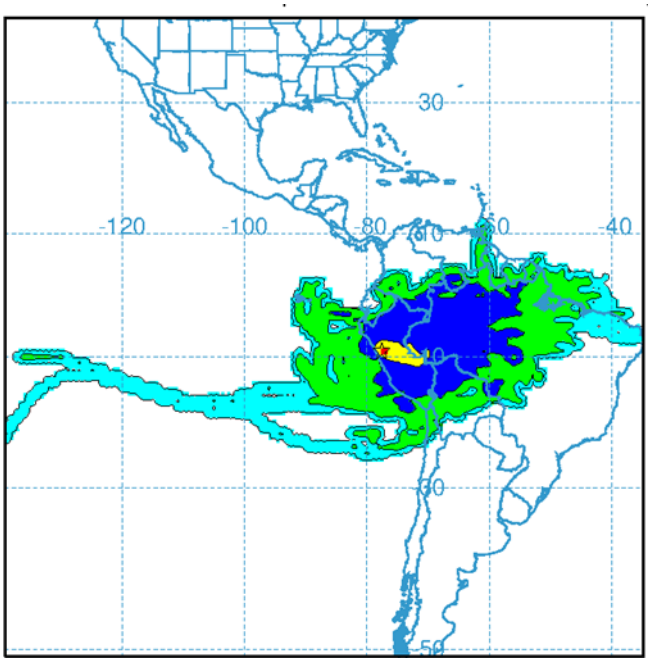

Figure 12: Seven day back trajectories during the wet season (1997-1998) under El Niño conditions

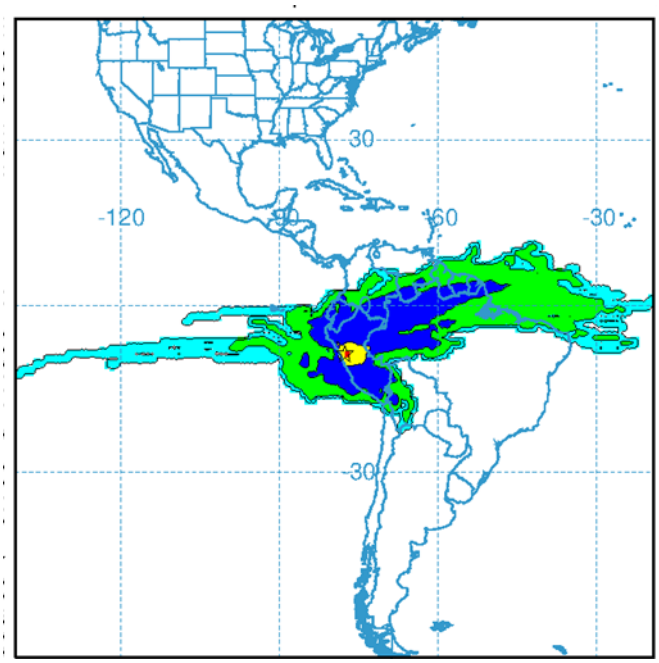

Figure 13: Seven day back trajectories during the wet season (2009-2010) under El Niño conditions

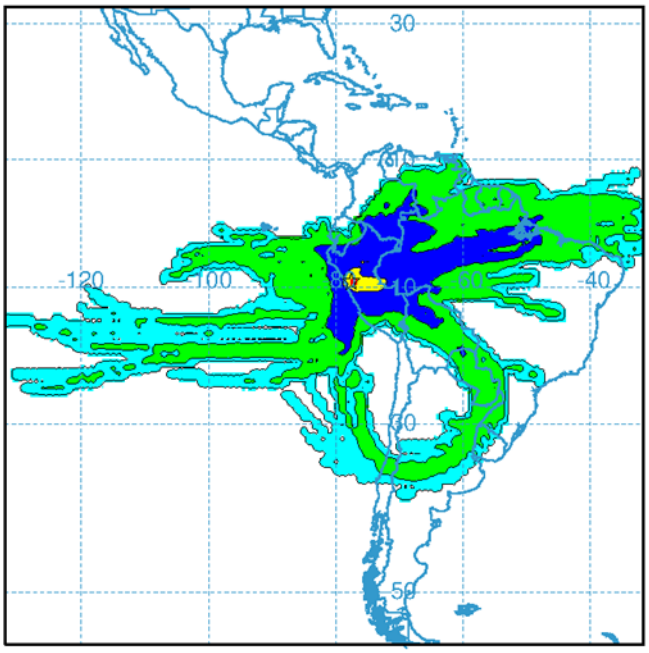

Figure 14: Seven day back trajectories during the wet season (2015-2016) under El Niño conditions

The trajectories for the wet seasons discussed above are shown below using the cluster analysis that groups the frequencies into 4 groups representing the four cardinal directions. This simplifies the figure and facilitates synthesis of the air mass tracks. Figure 15 shows an example of neutral conditions in the wet season of 2001-2002, Figure 16 shows an example of La Niña conditions in the wet season of 1998-1999, and Figures 17-19 show the El Niño conditions of the wet seasons of 1997-1998, 2009-2010, and 2015-2016, respectively. The cluster analyses are from 72 hour trajectories. The clusters are summarized by the direction of origin in Table 6.

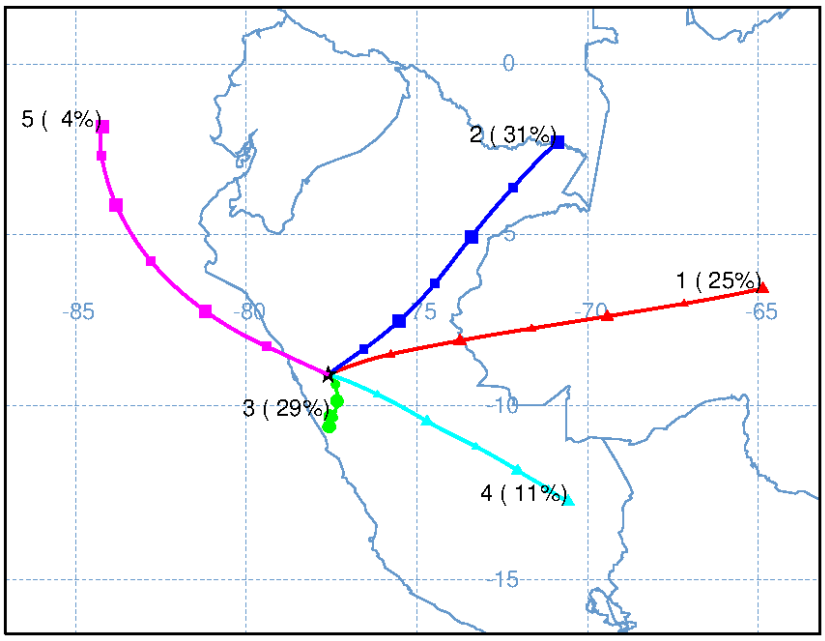

Figure 15: Three day back trajectories during the wet season (2001-2002) under neutral ENSO conditions

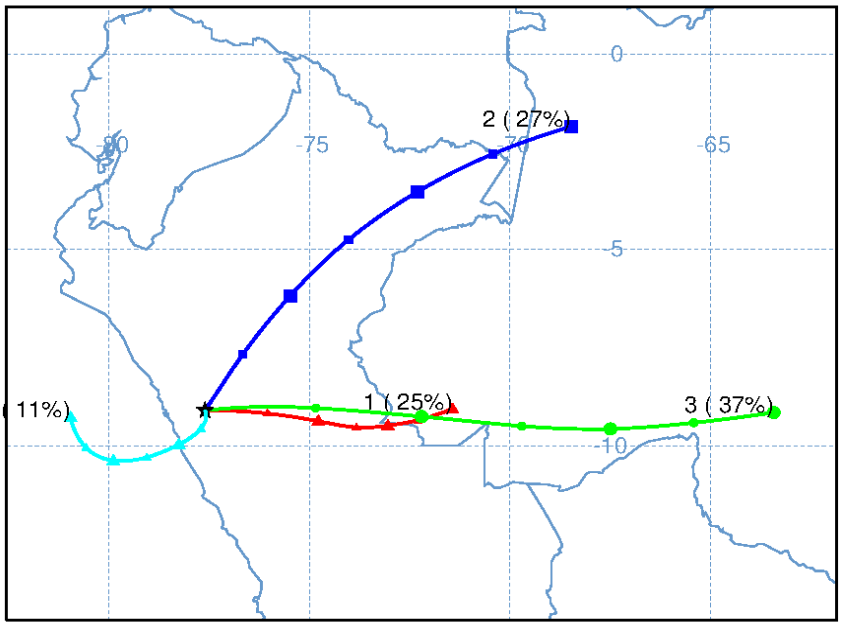

Figure 16: Three day back trajectories during the wet season (1998-1999) under La Niña conditions

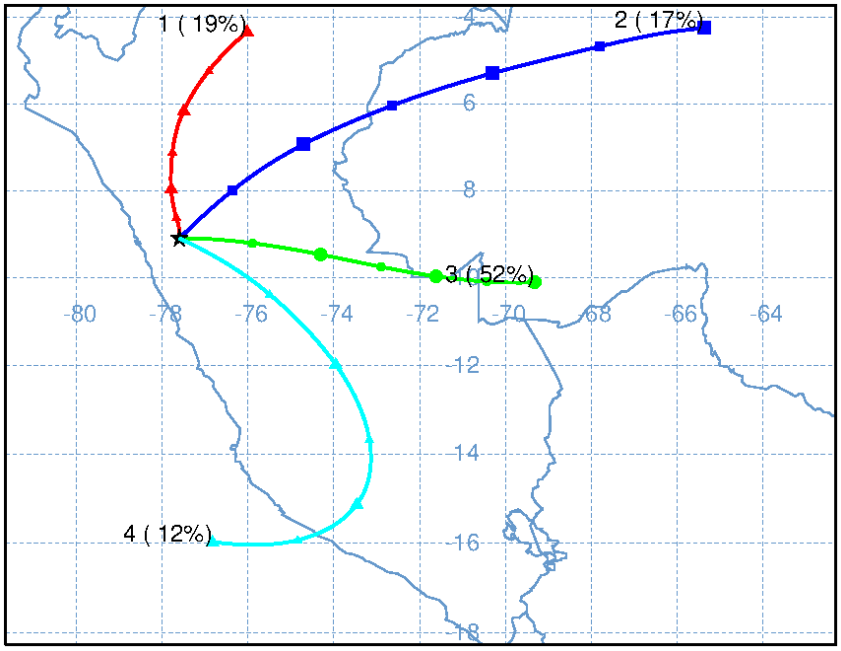

Figure 17: Three day back trajectories during the wet season (1997-1998) under El Niño conditions

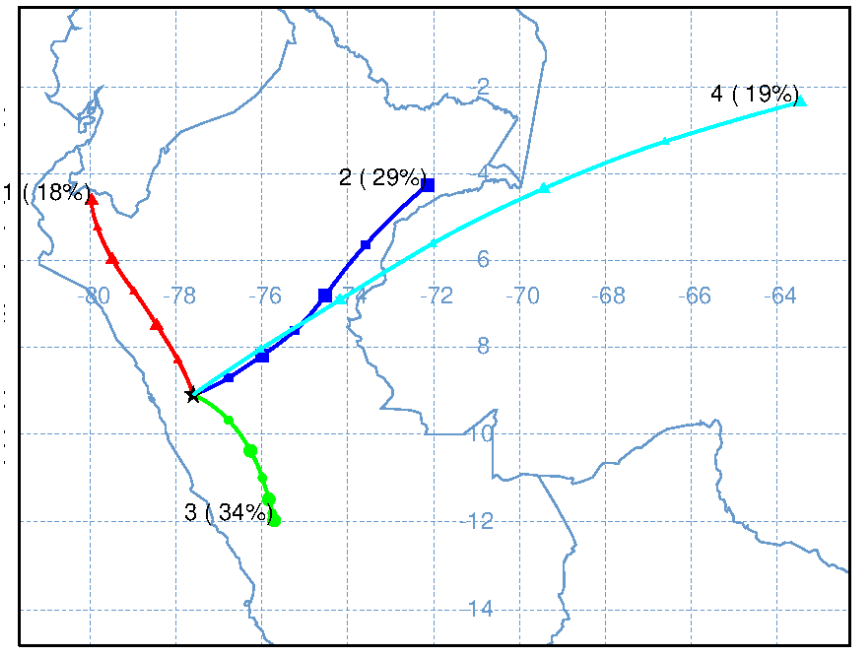

Figure 18: Three day back trajectories during the wet season (2009-2010) under El Niño conditions

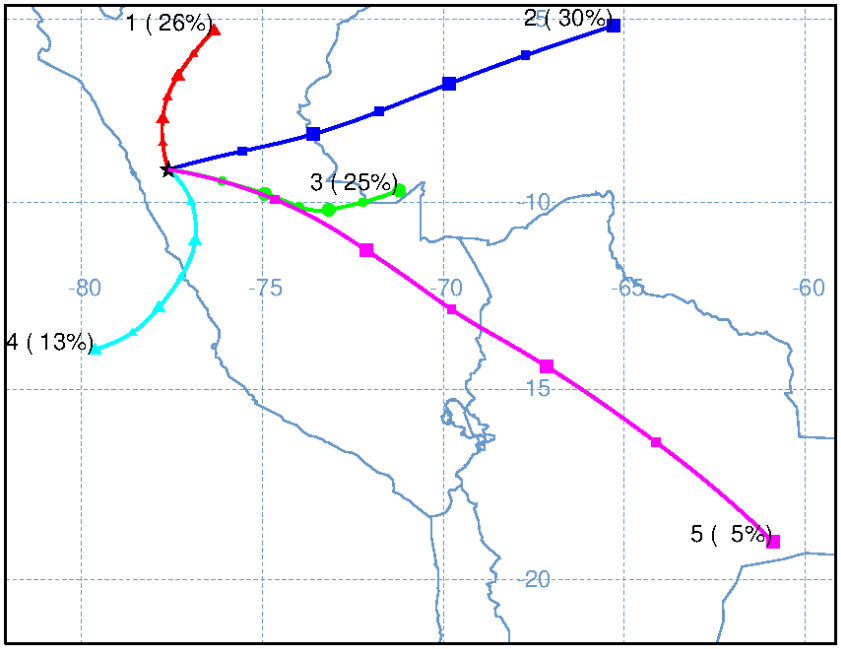

Figure 19: Three day back trajectories during the wet season (2015-2016) under El Niño conditions

The cluster analyses generally show more easterly circulation during La Niña events and less during El Niño events. The other more surprising result is the split of the trajectories between north and south for those that do not come from the east during the El Niño and neutral years, whereas in La Niña years, almost all circulation that is not from the east comes from the west. This lack of direct western air mass origin points to a more complex reason for the isotopic correlation with central Pacific SSTs at Huascarán than simple airflow from this

region during El Niño events, such as the "atmospheric bridge" discussed by Henderson et al. (1999).

Table 6: Summary of cluster analyses. This table shows the percent of the trajectories originating from each cardinal direction.

Year	% of trajectories originating from N	% of trajectories originating from S	% of trajectories originating from W	% of trajectories originating from E
1997	19	12	0	69
2009	18	34	0	48
2015	26	13	0	61
2001	4	29	0	67
2003	23	0	0	77
2013	25	27	0	48
1998	0	0	11	89
1999	15	0	0	85
2007	0	0	18	82
2010	23	0	19	58

3.6. Reanalysis modeled climate data

Modeled upper tropospheric temperatures at Huascarán correlated very significantly with Pacific SSTs, particularly at the 200 and 500 mb regions in the NIÑO3.4 region, at the 500 mb level with the NIÑO4 region, and at the 200 mb level in the NIÑO3 and SOI regions. Table 6 shows the correlations between upper tropospheric temperatures and SSTs in the different NIÑO regions.

All of the following correlations in the chart are significant at $p<0.001$.

Table 7: Correlations between SSTs and pressure in the Pacific and upper tropospheric temperatures at Huascarán.

temperature in atmosphere at elevation (mb)	NIÑO4	NIÑO3.4	NIÑO3	NIÑO1+2	SOI
500	0.883	0.886	0.818	0.600	-0.860
400	0.770	0.836	0.823	0.689	-0.788
300	0.674	0.787	0.811	0.734	-0.720
250	0.731	0.838	0.854	0.765	-0.775
200	0.839	0.910	0.898	0.781	-0.891
150	0.765	0.789	0.762	0.619	-0.821

The link between 500 mb temps and $\delta^{18}O$ ($r = 0.618$, $p < 0.001$) was slightly weaker than that between $\delta^{18}O$ and NIÑO4. There were strong positive correlations ($r = \sim 0.6$) between upper tropospheric temperatures and isotopic ratios at the 200 and 500 mb levels for both $\delta^{18}O$ and δD. If the mechanism through which these upper tropospheric temperatures correlate with central Pacific SSTs can be determined, this could present a pathway through which SSTs could influence the isotopic values at Huascarán. Henderson et al. (1999) discussed a 500 mb connection through which central Pacific SSTs influence the wind

vectors in the tropical South Atlantic through the weakening of the Easterlies, and Hurley et al. (2019) discussed how differences in circulation patterns due to ENSO can result in isotopic depletion in the Andes. However, these explanations do not explain the very strong correlations between central Pacific SSTs and upper air temperatures at the 200 and 500 mb levels. However, they could present an additional factor that leads to the strong connection with central Pacific SSTs: perhaps both the increased upper atmospheric temperatures above Huascarán and the lower levels of Amazonian precipitation before Atlantic air reaches Huascarán have an impact on the isotopic signal recorded in the ice core.

Another possible factor which may be linked with upper atmospheric temperature may be cloud echo top height: Scholl et al. (2009) found that in eastern Puerto Rico, the isotopic composition of rainfall is influenced by cloud heights, which in turn are influenced by atmospheric temperature and seasonal climate patterns.

Outgoing longwave radiation (OLR) at Huascarán correlated more strongly with $\delta^{18}O$ and δD than did any of the Pacific NIÑO indices ($r = 0.693$ and 0.689, $p<0.001$ for $\delta^{18}O$ and δD, respectively). Samuels-Crow et al. (2014) found a strong relationship between upwind OLR and δD in the tropical Andes, from which they argue that tropical convection rather than temperature exerts a primary control over $\delta^{18}O$ of snow in the Andes but they did not study OLR at the site of precipitation. However, they mention numerous ways in which Pacific SSTs associated with ENSO influence convective intensity upwind of the Andes, including many of those discussed in this study: ITCZ position, Hadley Circulation strength, Atlantic SSTs, South American precipitation, and Altiplano climate.

The factors behind the isotopic signal of ENSO at Huascarán are likely complex, but the strong correlation between NIÑO4 SSTs and $\delta^{18}O$ and δD indicates that this is a robust signal which may be used in paleoclimate research. Examination of lower atmospheric temperatures might have been useful in understanding the patterns in effect here; however, they were excluded from this study because the col of Huascarán is typically located around or above the 500 mb level.

4. Summary/Conclusions

This study investigates possible ENSO-linked patterns in the data from 1994-2019 in the ice cores from the col of Huascarán Mountain in the Cordillera Blanca, Peru. Consistent with previous research (Henderson, 1996), the strongest relationship is with the isotopic records. The correlations between $\delta^{18}O$ and δD with NIÑO4 are 0.682 and 0.672 ($p<0.001$), respectively. This strong isotopic signal may be linked to Amazonian precipitation patterns that shift with ENSO (Vuille et al., 2019) or with echo top heights of clouds (Scholl et al., 2009). Alternatively, or additionally, this connection may be linked to the OLR at Huascarán or the strong relationship between Pacific SSTs and the upper tropospheric temperatures at Huascarán.

Net accumulation exhibits a weak but significant ($r=-0.451$, $p=0.021$) negative relationship with NIÑO4 SSTs, which may be indicative of a northward migration of the area of ENSO-linked drought in Peru, or which may simply be a product of the three El Niño events in this 25-year study. Dust does not significantly correlate with Pacific ENSO indices, but it does significantly correlate with Atlantic SSTs; correlation with the AMO was significant ($r=0.574$, $p=0.002$). Future study of the dust's origin through analysis of its chemical composition may help to explain the Atlantic modulation of its concentration at Huascarán. Sulfate concentrations are significantly lower ($p=0.033$) during El Niño years than in La Niña or neutral years, but do not exhibit a significant relationship with any of the Pacific SST indices. The origin of this sulfate signal is unknown, but its presence or absence deeper in the core should reveal whether it is natural or anthropogenic. Deuterium excess is negatively correlated with NIÑO1+2 SSTs ($r=-0.470$, $p=0.016$), but exclusion of the 1997-1998 East Pacific (EP) El Niño event significantly weakens the relationship. Investigation of this signal deeper in the core where that are more occurrences of EP events is essential to assess the significance of this relationship.

5. Acknowledgements

I would like to thank Drs. Ellen Mosley-Thompson and Lonnie Thompson for serving as my advisors on this project and for their support throughout my undergraduate education. Ellen first introduced me to paleoclimatology in her class, helped me get involved at the Byrd Polar and Climate Research Center, and then took me into her lab, where I have benefitted in countless ways from the guidance, support, and inspiration provided by her, Lonnie, and the rest of the BPCRC-ICPRG.

I would like to thank Drs. Emilie Beaudon, Stacy Porter, and Roxana Sierra-Hernández for working closely with me throughout my time at Byrd and for introducing me to so many different facets of ice core paleoclimatology research.

I would like to thank all of the above as well as Dr. Mary Davis for their continued support, guidance, insight, and solutions to problems throughout this thesis project. I am so grateful to all of you!

I would like to thank Dr. Becky Mansfield for her support and guidance throughout my undergraduate education, for introducing me to science studies, and for serving on my thesis committee.

I thank Donald Kenny for the dust and ion analyses, Dr. Ping-Nan Lin for the isotope analyses, and the BPCRC-ICPRG field team for ice core extraction. The ice core drilling and analyses were supported by NSF project 1805819.

Finally, I would like to thank my family and friends for their support throughout this project. In particular I would like to thank Dave, Sally, and Michael Bayless, Sophia Abukamail, Sofia Biegeleisen, James Li, Anna Leatherwood, Katherine Manifold, and Adele Purdy.

6. Works cited

All, J., Medler, M., Arques, S., Cole, R., Woodall, T., King, J., Yan, J. & Schmitt, C. (2017). Fire response to local climate variability: Huascarán National Park, Peru. *Fire Ecology, 13*(2), 85–104. https://doi: 10.4996/fireecology.130288764

Arnaud, Y., & Muller., F. (2001). El Niño-Southern Oscillation (ENSO) influence on a Sajama volcano glacier (Bolivia) from 1963 to 1988 as seen from Landsat data and aerial photography. *Journal of Geophysical Research, 106* (D16), 17,773-17,784.

Banholzer, S., & Donner, S. (2014). The influence of different El Niño types on global average temperature. *Geophysical Research Letters, 41,* 2093–2099, https://doi:10.1002/2014GL059520.

Bradley R.S., Vuille, M., Hardy, M., & Thompson, L.G. (2003). Low latitude ice cores record Pacific SSTs. *Geophysical Research Letters, 30*(3), 1774. https://doi:10.1029/2002GL016546.

Bird, B., Abbott, M., Vuille, M., Rodbell, D., Stansell, N., & Rosenmeier, M. (2011). A 2,300-year-long annually resolved record of the South American summer monsoon from the Peruvian Andes. *Proceedings of the National Academy of Sciences of the United States of America, 108,* 8583-8588. https://doi.org10.1073/pnas.1003719108.

Davis, M.E., L.G. Thompson, E. Mosley-Thompson, P.-N. Lin, V.N. Mikhalenko, & J. Dai. (1995). Recent ice-core climate records from the Cordillera Blanca, Peru. *Annals of Glaciology*, *21*, 225-230.

da Rocha Ribeiro, R., Simões, J.C., Ramirez, E. et al. (2018). Accumulation rate in a tropical Andean glacier as a proxy for northern Amazon precipitation. *Theoretical and Applied Climatology, 132*, 569–578. https://doi.org/10.1007/s00704-017-2108-7

Dansgaard, W. (1964). Stable isotopes in precipitation. *Tellus, 16*, 436-468. https://doi.org/10.1111/j.2153-3490.1964.tb00181.x

Fasullo, J. T., Otto-Bliesner, B. L., & Stevenson, S. (2018). ENSO's changing influence on temperature, precipitation, and wildfire in a warming climate. *Geophysical Research Letters, 45,* 9216– 9225. https://doi.org/10.1029/2018GL079022

Feng, M., McPhaden, M., Xie, S.P. et al. (2013). La Niña forces unprecedented Leeuwin Current warming in 2011. *Scientific Reports, 3,* 1277. https://doi.org/10.1038/srep01277

Henderson, K.A., Thompson, L.G., & Lin, P-N. (1999). Recording of El Niño in ice core δ18O records from Nevado Huascarán, Peru. *Journal of Geophysical Research, 104*(D24), 31,053-31,065.

Henderson, K.A. (1996). *The El Niño-Southern Oscillation and Other Modes of Interannual Tropical Climate Variability as Recorded in Ice Cores from the Nevado Huascarán Col, Peru* (Unpublished master's thesis). Ohio State University.

Hurley, J.V., Vuille, M., & Hardy, D.R. (2019). On the interpretation of the ENSO signal embedded in the stable isotopic composition of Quelccaya Ice Cap, Peru. *Journal of Geophysical Research: Atmospheres, 124,* 131– 145. https://doi.org/10.1029/2018JD029064

Garreaud R.D., Vuille M, Compagnucci R.H., & Marengo J. (2009). Present day South American climate. *Palaeogeography, Palaeoclimatology, Palaeoecology, 281,* 180–195.

Gierach, M.M., Lee, T., Turk, D., & McPhaden, M.J. (2012). Biological response to the 1997-98 and 2009-10 El Niño events in the equatorial Pacific Ocean. *Geophysical Research Letters, 39*(10), L10602, https://doi: 10.1029/2012GL051103.

Kim, W., Yeh, S.-W., Kim, J.-H., Kug, J.-S., & Kwon, M. (2011). The unique 2009–2010 El Niño event: A fast phase transition of warm pool El Niño to La Niña. *Geophysical Research Letters,* 38, L15809, httsp://doi:10.1029/2011GL048521.

Knüsel, S., .Brutsch, S. Henderson, K., Palmer, A., & Schwikowski, M. (2005). ENSO signals of the twentieth century in an ice core from Nevado Illimani, Bolivia. *Journal of Geophysical Research, 110* (D1). https://doi: 10.1029/2004jd005420.

Lindsey, R. (2016, August 2). (2015). State of the Climate: El Niño came, saw, and conquered. Climate.Gov. https://www.climate.gov/news-features/understanding-climate/2015-state-climate-el-ni%C3%B1o-came-saw-and-conquered

Liu, W., & Xie, S.-P. (2018). An ocean view of the global surface warming hiatus. *Oceanography, 31*(2), 72–79. https://doi.org/10.5670/oceanog.2018.217

L'Heureux, M. (2008). An Overview of the 2007- 08 La Niña and Boreal Wintertime Variability. *Science and Technology Infusion Climate Bulletin, NOAA's National Weather Service.* https://www.nws.noaa.gov/ost/climate/STIP/33CDPW/LHeureux_33cdpw.htm#:~:text=According%20to%20the%20ONI%2C%20the,April%2DMay%2DJune%202008.&text=The%20seasonal%20mean%20anomalies%20for,a%20strong%20La%20Niña%20episode.

McPhaden M.J. (1999). Genesis and evolution of the 1997-98 El Niño. *Science*. *283*(5404), 950-954. https://doi.org/10.1126/science.283.5404.950.

McPhaden, M.J., Santoso, A. and Cai, W. (2020). Introduction to El Niño Southern Oscillation in a Changing Climate. In *El Niño Southern Oscillation in a Changing Climate*. Hoboken, NJ: Wiley-American Geophysical Union. Edited by M.J. McPhaden, A. Santoso and W. Cai. https://doi.org/10.1002/9781119548164.ch1

NOAA. (n.d.). *Equatorial Pacific Sea Surface Temperatures | Teleconnections | National Centers for Environmental Information (NCEI)*. Equatorial Pacific Sea Surface Temperatures | Teleconnections. Retrieved April 4, 2021, from https://www.ncdc.noaa.gov/teleconnections/enso/indicators/sst/

Paek, H., Yu, J.-Y., & Qian, C. (2017). Why were the 2015/2016 and 1997/1998 extreme El Niños different? *Geophysical Research Letters, 44*. https://doi:10.1002/2016GL071515.

Rocha, V., Teixeria, P. R., Gomes, W., Vergasta, L., & Jardin, A. (2018). Precipitation Recycling in the Amazon Basin: A Study Using the ECMWF Era-Interim Reanalysis Dataset. *Geography Department University of Sao Paulo, 35,* 71-82. https://doi.10.11606/rdg.v35i0.139494.

Rolph, G., Stein, A., & Stunder, B. (2017). Real-time Environmental Applications and Display System: READY. *Environmental Modelling & Software, 95,* 210-228, https://doi.org/10.1016/j.envsoft.2017.06.025

Rupic, M., Wetzell, L., Marra, J. J., & Balwani, S. (2018). 2014-2016 El Niño assessment report: An overview of the impacts of the 2014-16 El Niño on the U.S.-affiliated Pacific Islands (USAPI). NOAA National Centers for Environmental Information, Honolulu, HI.

Samuels-Crow, K. E., Galewsky, J., Hardy, D. R., Sharp, Z. D., Worden, J., & Braun, C. (2014). Upwind convective influences on the isotopic composition of atmospheric water vapor over the tropical Andes. *Journal of Geophysical Research: Atmospheres, 119,* 7051– 7063. https://doi:10.1002/2014JD021487.

Scholl, M. A., Shanley, J. B., Zegarra, J. P., and Coplen, T. B. (2009). The stable isotope amount effect: New insights from NEXRAD echo tops, Luquillo Mountains, Puerto Rico. *Water Resources Research, 45,* W12407. doi:10.1029/2008WR007515.

Shabbar, A., & B. Yu (2009). The 1998–2000 La Niña in the context of historically strong La Niña events. *Journal of Geophysical Research, 114,* D13105. https://doi:10.1029/2008JD011185.

Stein, A.F., Draxler, R.R, Rolph, G.D., Stunder, B.J.B., Cohen, M.D., & Ngan, F. (2015). NOAA's HYSPLIT atmospheric transport and dispersion modeling system. *Bulletin of the American Meteorological Society, 96,* 2059-2077. http://doi.org/10.1175/BAMS-D-14-00110.1

Stockdale, T., Balmaseda, M. & Ferranti, L. (2017). The 2015/2016 El Niño and beyond. *ECMWF Newsletter, 151,* 16-21.

Sulca, J.,Takahashi, K., Espinoza, J., Vuille, M., & Lavado, W. (2017). Impacts of different ENSO flavors and tropical Pacific convection variability (ITCZ, SPCZ) on austral summer rainfall in South America, with a focus on Peru. *International Journal of Climatology.* https://doi.10.1002/joc.5185.

Thompson, L.G., Mosley-Thompson. E., & Arnao, B.M. (1984). Major El Niño-Southern Oscillation events recorded in stratigraphy of the tropical Quelccaya Ice Cap. *Science, 226*(4670), 50-52.

Thompson, L.G., E. Mosley-Thompson. J.F. Bolzan & B.R. Koci. (1986). A 1500 year record of climate variability recorded in ice cores from the tropical Quelccaya Ice Cap. *Science, 229*(471), 971-973

Thompson, L.G., E. Mosley-Thompson & P.A. Thompson. (1992). Reconstructing interannual climate variability from tropical and subtropical ice-core records. Chapter 16 In: H. Diaz and V. Markgraf (Eds.), *El Niño, Historical and Paleoclimatic Aspects of the Southern Oscillation,* Cambridge University Press, 295-322.

Thompson, L.G., Mosley-Thompson, E., Davis, M.E., Lin, P-N., Henderson, K.A., Cole-Dai, J., Bolzan J.F., & Liu, K.-B. (1995). Late Glacial Stage and Holocene tropical ice core records from Huascarán, Peru. *Science, 269,* 46-50.

Thompson, L. G., Mosley-Thompson, E., Davis, M.E., Zagorodnov, V.S., Howat,I.M., Mikhalenko, V.N., & Lin, P.-N. (2013). Annually resolved ice core records of tropical climate variability over the past ~1800 years. *Science, 340*(6135), 945-950.

Thompson, L. G., Davis, M. E., Mosley-Thompson, E., Beaudon, E., Porter, S. E., Kutuzov, S., Lin, P.-N., Mikhalenko, V. N., & Mountain, K. R. (2017). Impacts of recent warming and the 2015/16 El Niño on tropical Peruvian ice fields. *Journal of Geophysical Research: Atmospheres, 122*. https://doi.org/10.1002/2017JD026592.

Trenberth, K. E., Caron, J. M., Stepaniak, D. P., & Worley, S. (2002). Evolution of El Niño–Southern Oscillation and global atmospheric surface temperatures. *Journal of Geophysical Research, 107*(D8). https://doi.org/10.1029/2000JD000298

Villavicencio Guillén, E. E. (2019). Datos de precipitación y temperatura en zonas de escasa información de la región Ancash—Periodo 2012-2017, 2019. (Unpublished master's thesis.) Santiago Antúnez de Mayolo National University.

Vuille, M., Bradley, R.S., Healy, R., Werner, R., Hardy, D. R., Thompson, L. G., & Keimig, F. (2003). Modeling δ18O in precipitation over the tropical Americas, Part II: Simulation of the stable isotope signal in Andean ice cores. *Journal of Geophysical Research: Atmospheres, 108*, https://doi.org/10.1029/2001JD002039

Zhang, R. H., Zheng, F., Zhu, J. et al. (2013). A successful real-time forecast of the 2010–11 La Niña event. *Scientific Reports, 3*, 1108. https://doi.org/10.1038/srep01108

Appendix

A1. Acronyms

AMO—Atlantic Multi-decadal Oscillation

CP—Central Pacific (type of El Niño event)

EP—Eastern Pacific (type of El Niño event)

ENSO—El Niño-Southern Oscillation

GPH—Geopotential Height

GPM—Global Precipitation Measurement

IPO—Inter-decadal Pacific Oscillation

ITCZ—Inter Tropical Convergence Zone

LGS—Last Glacial Stage

MSA—methane sulfonic acid, $CH_3SO_3^-$

ONI—Oceanic Niño Index

SOI—Southern Oscillation Index

SASM—South American Summer Monsoon

SMOW—Standard Mean Ocean Water

SOI—Southern Oscillation Index

SPCZ—South Pacific Convergence Zone

SSTs—sea surface temperatures

TNA—Tropical North Atlantic Index

TSA—Tropical South Atlantic Index

TRMM—Tropical Rainfall Measuring Mission

A2. Additional back trajectories

A2.1. Frequency trajectories

Frequency trajectories from the wet seasons of the La Niña events of 1999-2000, 2007-2008, and 2010-2011 are shown in Figures A1-A3 and the neutral conditions in 2003-2004 and 2013-2014 are shown in Figures A4-A5.

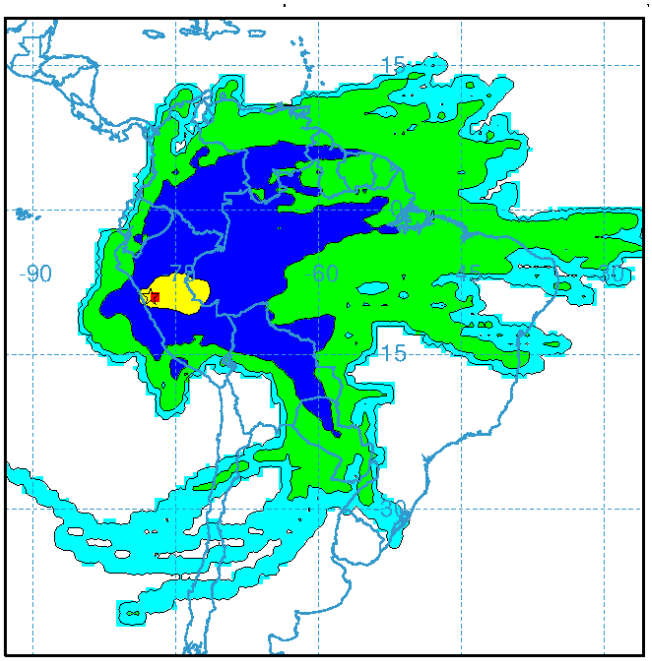

Figure A1: Seven day back trajectories during the wet season (1999-2000) under La Niña conditions

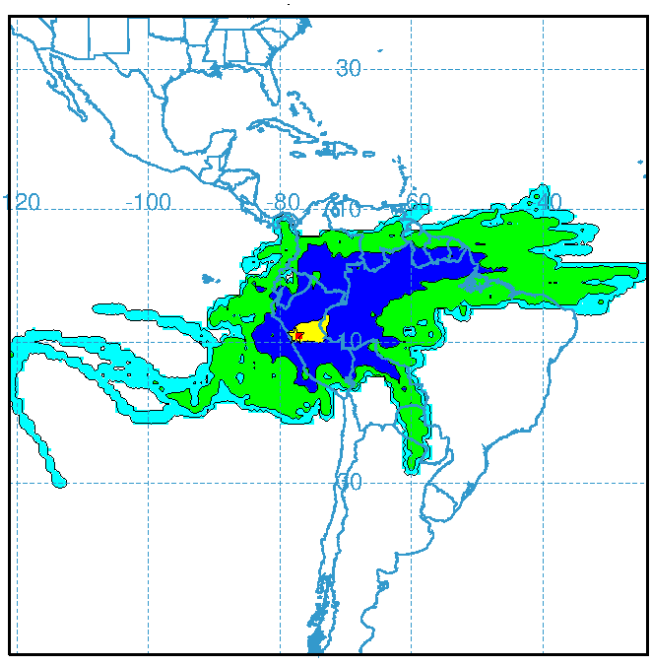

Figure A2: Seven day back trajectories during the wet season (2007-2008) under La Niña conditions

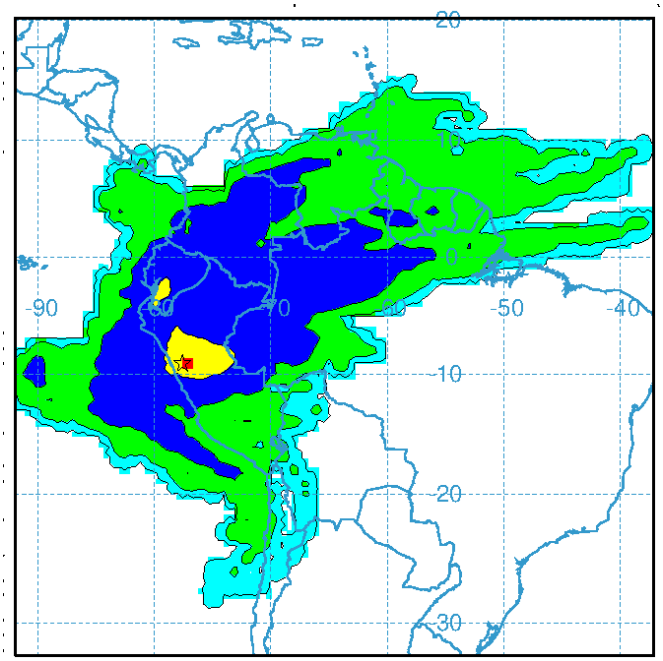

Figure A3: Seven day back trajectories during the wet season (2010-2011) under La Niña conditions

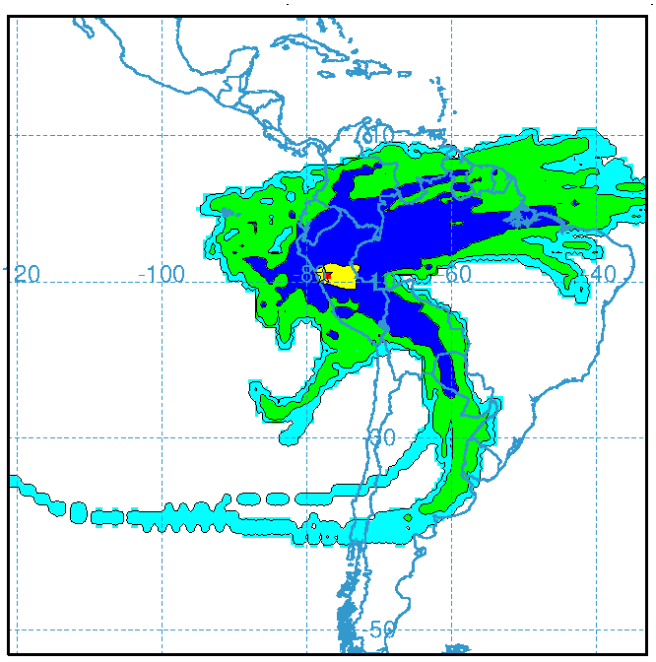

Figure A4: Seven day back trajectories during the wet season (2003-2004) under neutral ENSO conditions

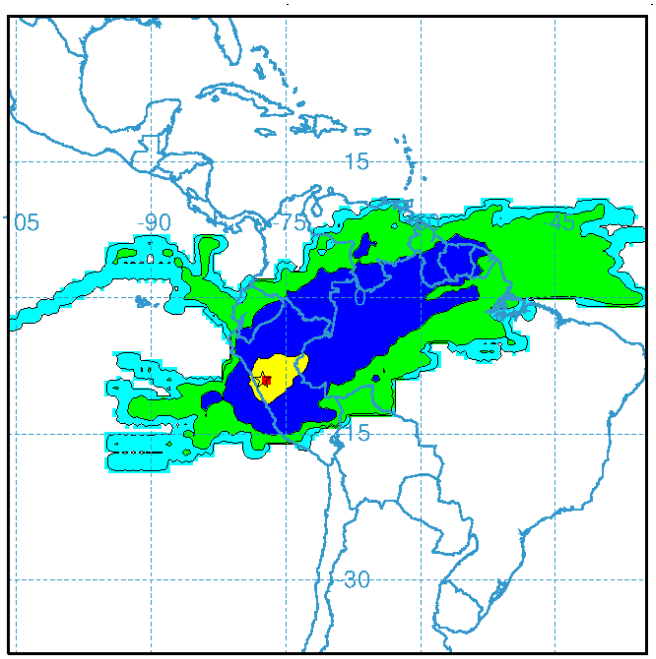

Figure A5: Seven day back trajectories during the wet season (2013-2014) under neutral ENSO conditions

A2.2. Clustered trajectories

Clusters of trajectories from the wet seasons of the La Niña events of 1999-2000, 2007-2008, and 2010-2011 are shown in Figures A6-A8 and the neutral conditions in 2003-2004 and 2013-2014 are shown in Figures A9-A10.

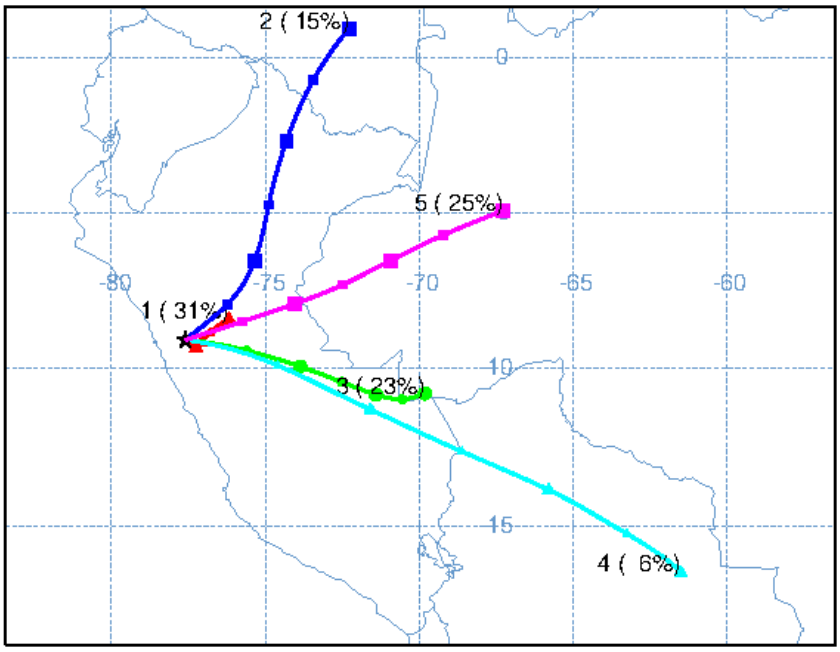

Figure A6: La Niña conditions in the wet season of 1999-2000

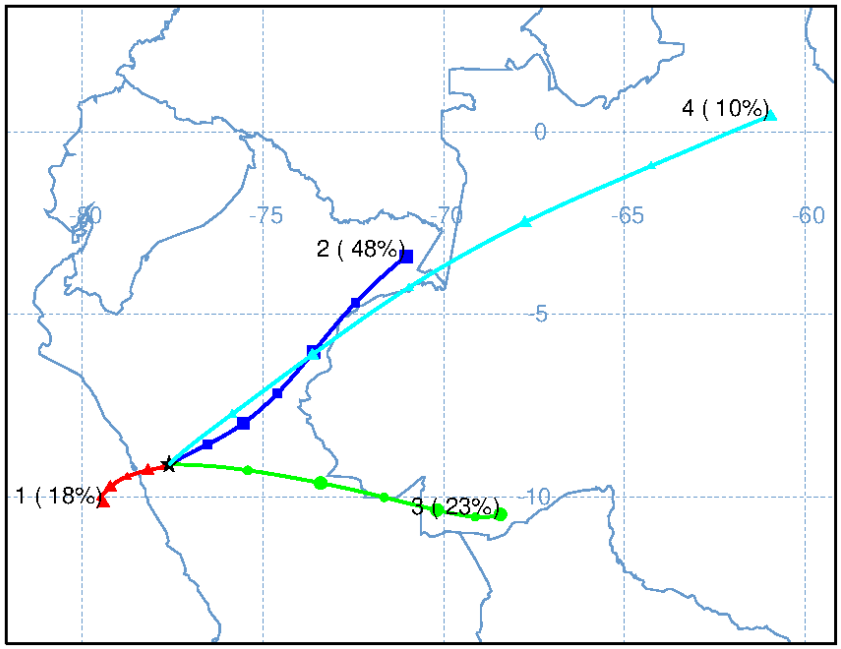

Figure A7: La Niña conditions in the wet season of 2007-2008

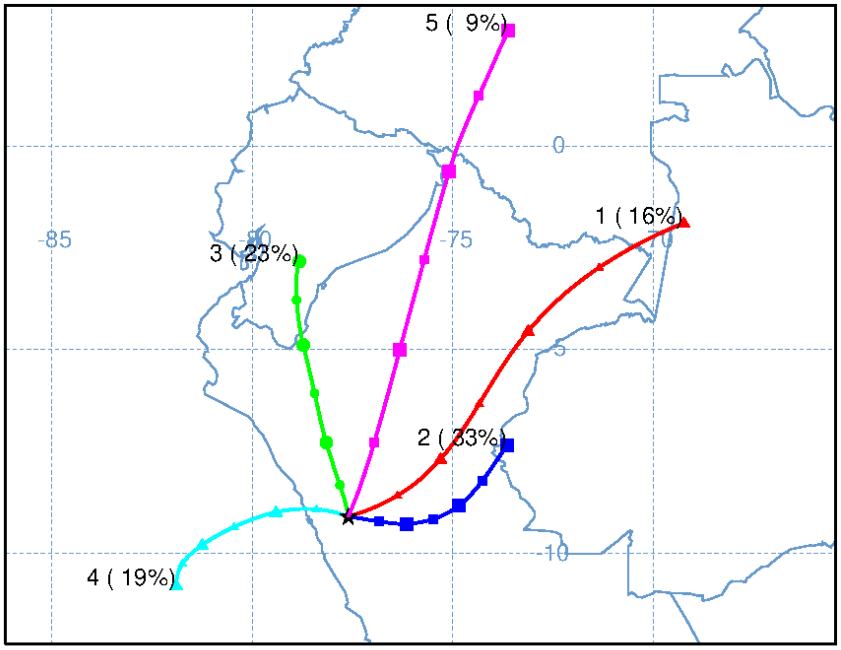

Figure A8: La Niña conditions in the wet season of 2010-2011

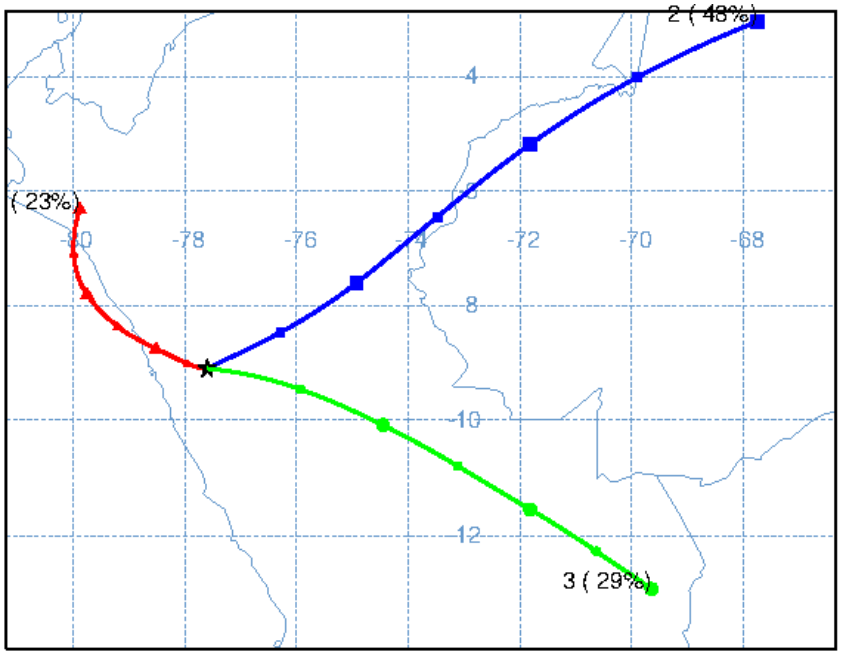

Figure A9: Neutral conditions in the wet season of 2003-2004

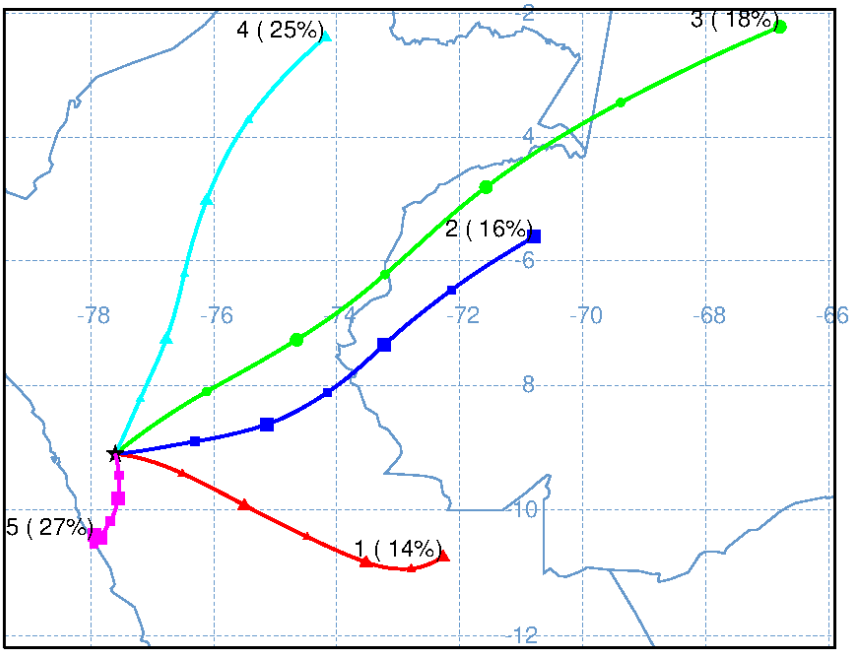

Figure A10: Neutral conditions in the wet season of 2013-2014

A2.3. Dry season trajectories

The following back trajectories show seven-day frequency plots from April-August of the calendar year specified. Figure A11 shows 1998, Figure A12 shows 1999, Figure A13 shows 2002, Figure A14 shows 2008, and Figure A15 shows 2010, and Figure A16 shows 2015.

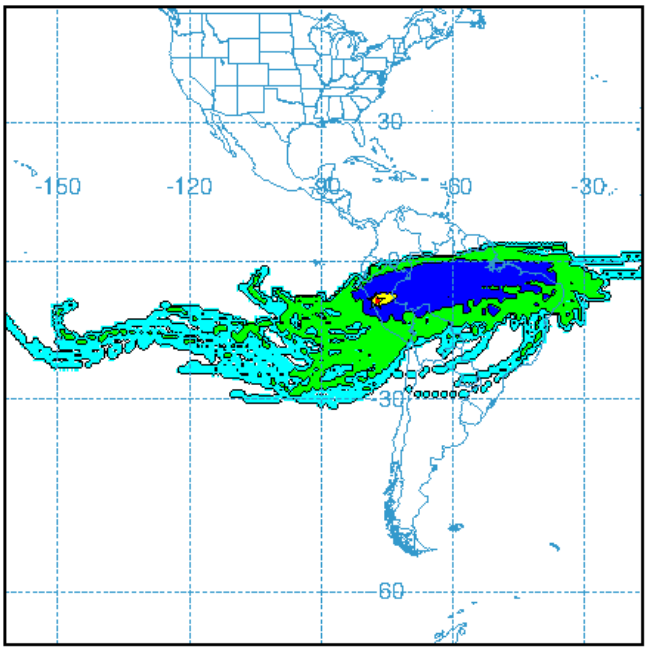

Figure A11: Seven day back trajectories during the dry season (1998) under the disintegration of El Niño conditions and onset of La Niña conditions

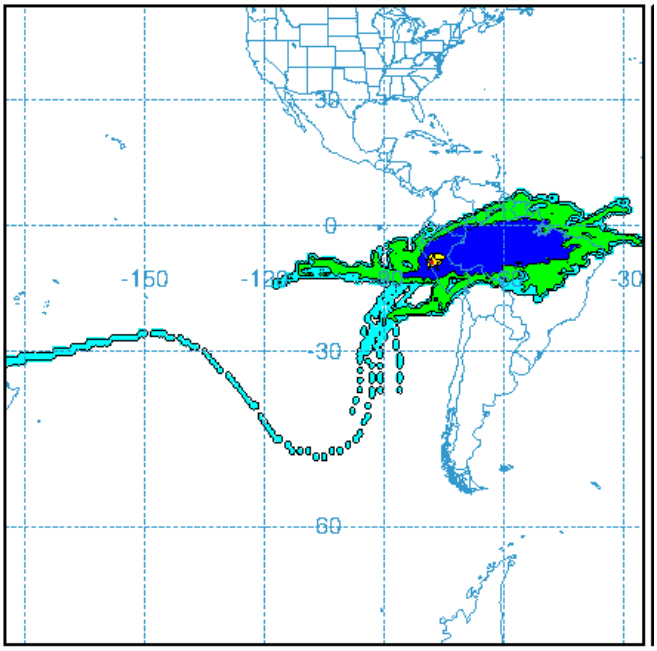

Figure A12: Seven day back trajectories during the dry season (1999) under strong La Niña conditions

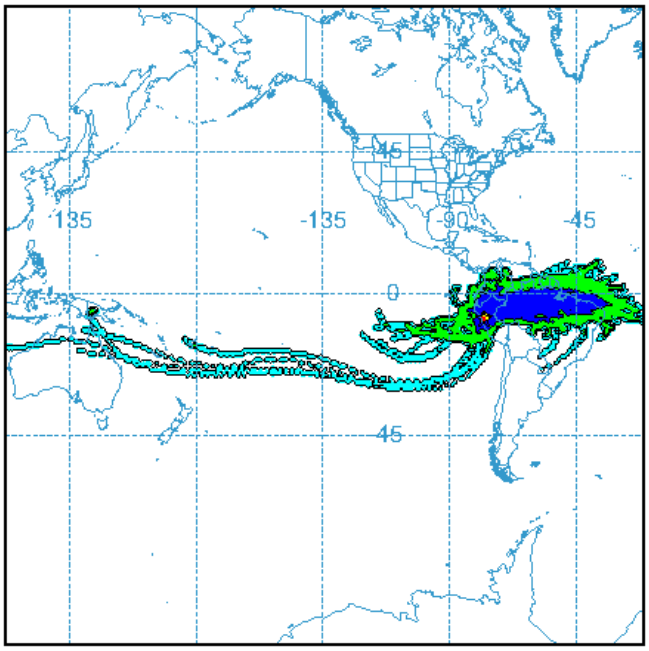

Figure A13: Seven day back trajectories during the dry season (2002) under the very neutral conditions

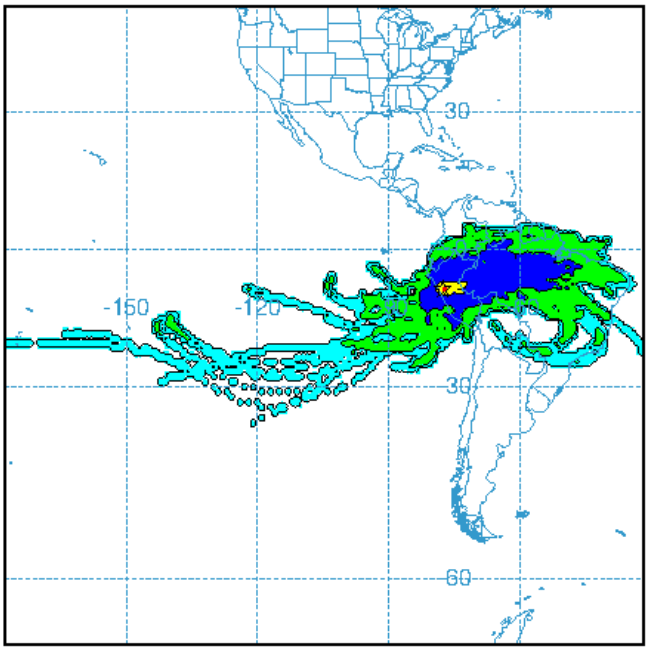

Figure A14: Seven day back trajectories during the dry season (2008) under moderate La Niña conditions

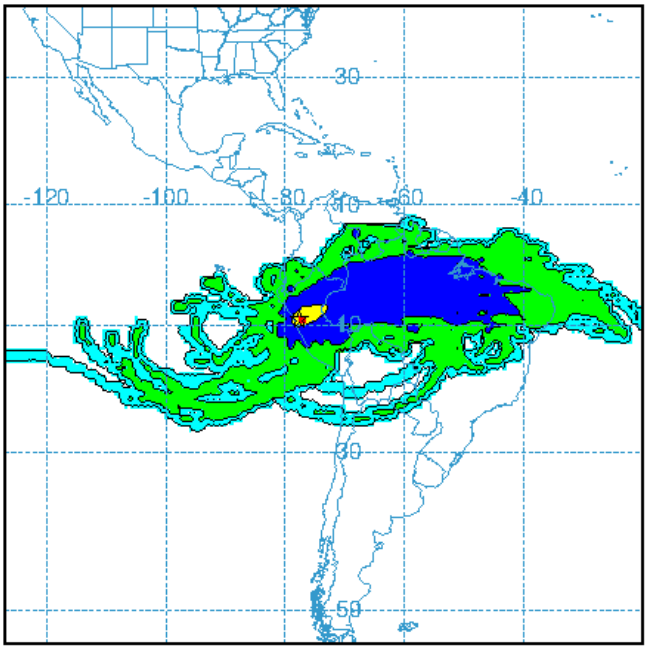

Figure A15: Seven day back trajectories during the dry season (2010) under the onset of La Niña conditions

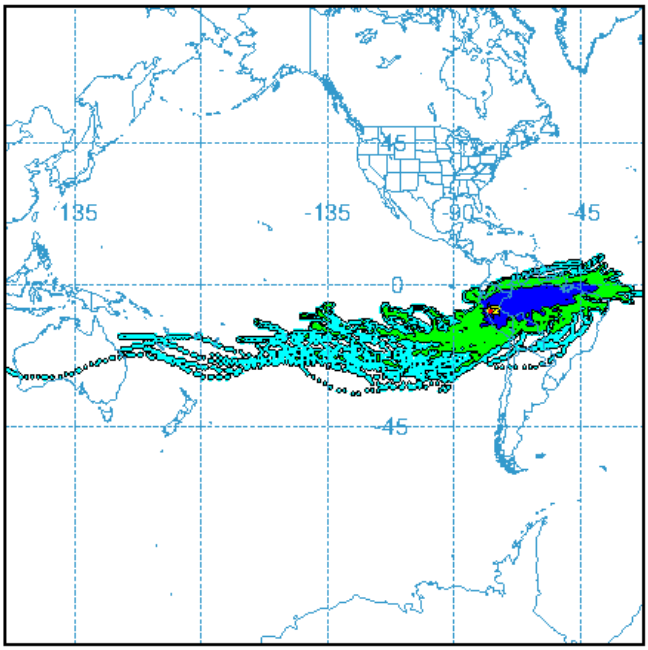

Figure A16 : Seven day back trajectories during the dry season (2015) under the El Niño conditions

A.2.4. Total spatial variance

The following plots of total spatial variance were used to determine the number of clusters best to use for each wet season. The number closest to five with the lowest total spatial variance between clustered trajectories was chosen.

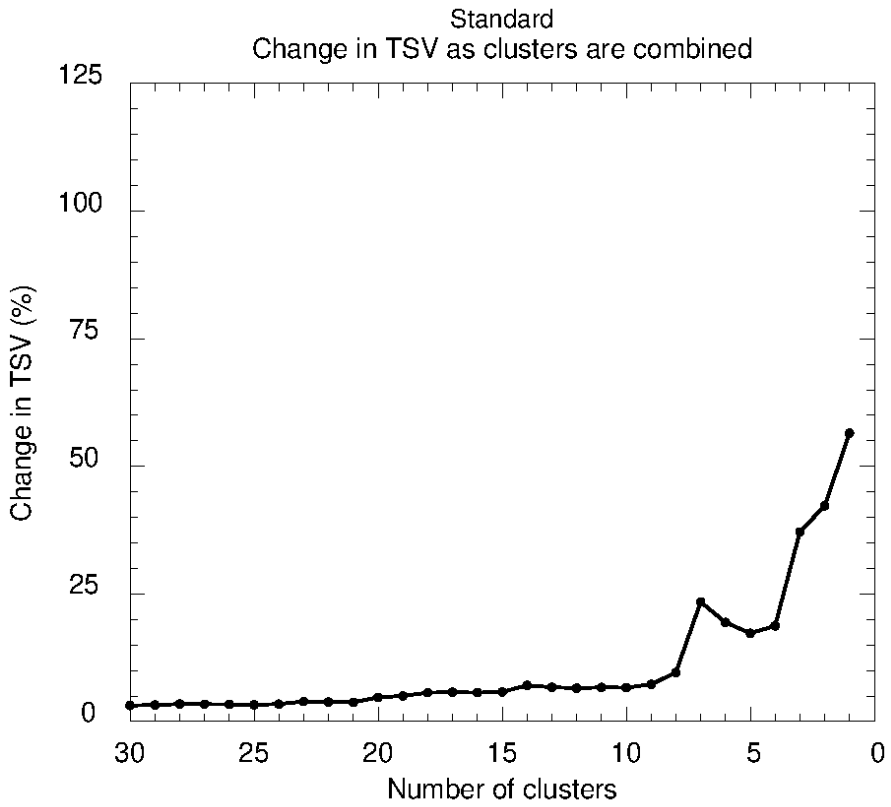

Figure A17: Total spatial variance for cluster analysis in the 1997-1998 El Niño (wet season)

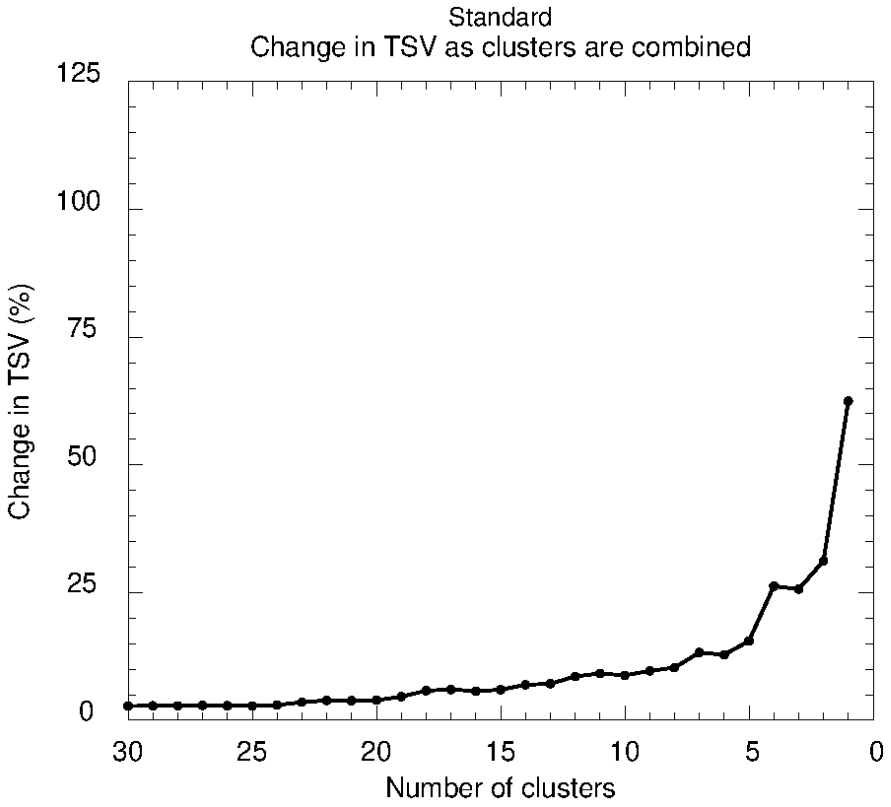

Figure A18: Total spatial variance for cluster analysis in the 1998-1999 La Niña (wet season)

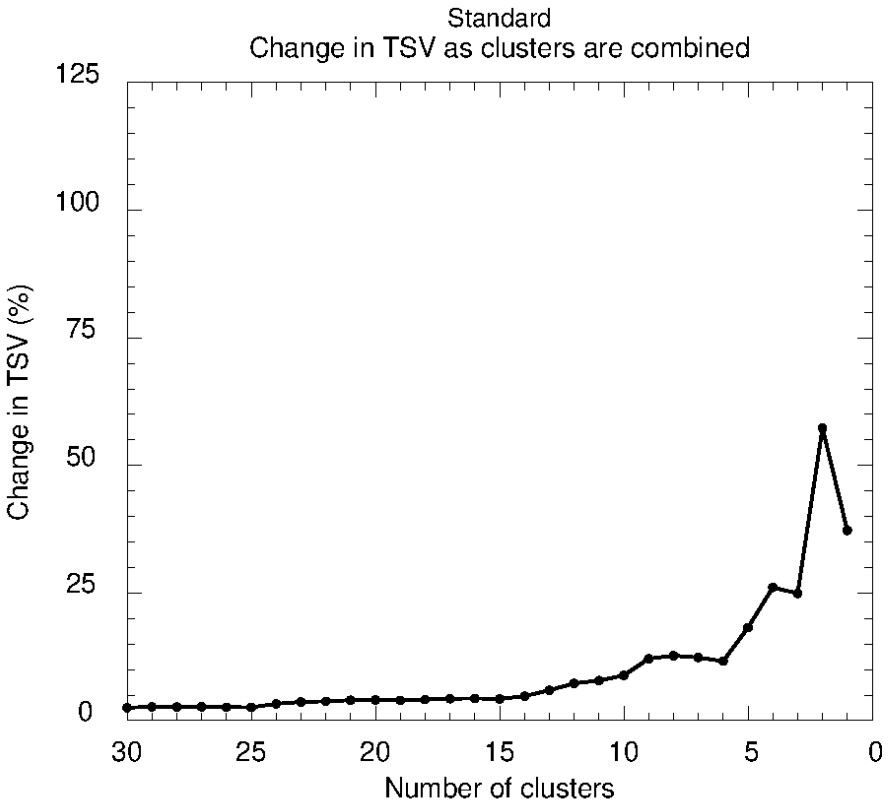

Figure A19: Total spatial variance for cluster analysis in the 1999-2000 La Niña (wet season)

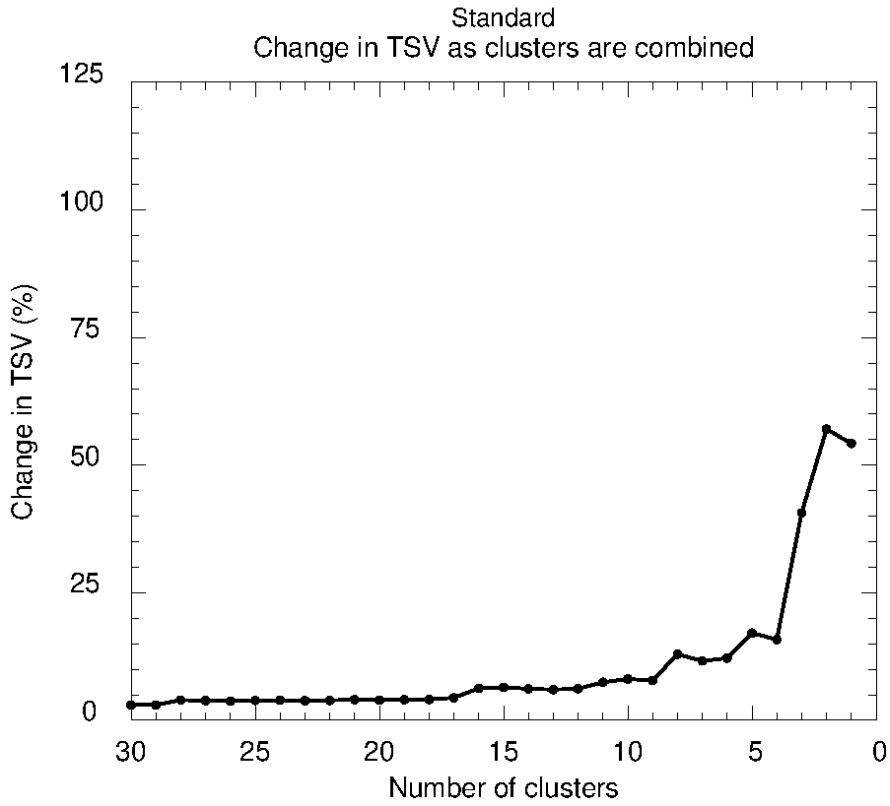

Figure A20: Total spatial variance for cluster analysis in the 2001-2002 neutral wet season

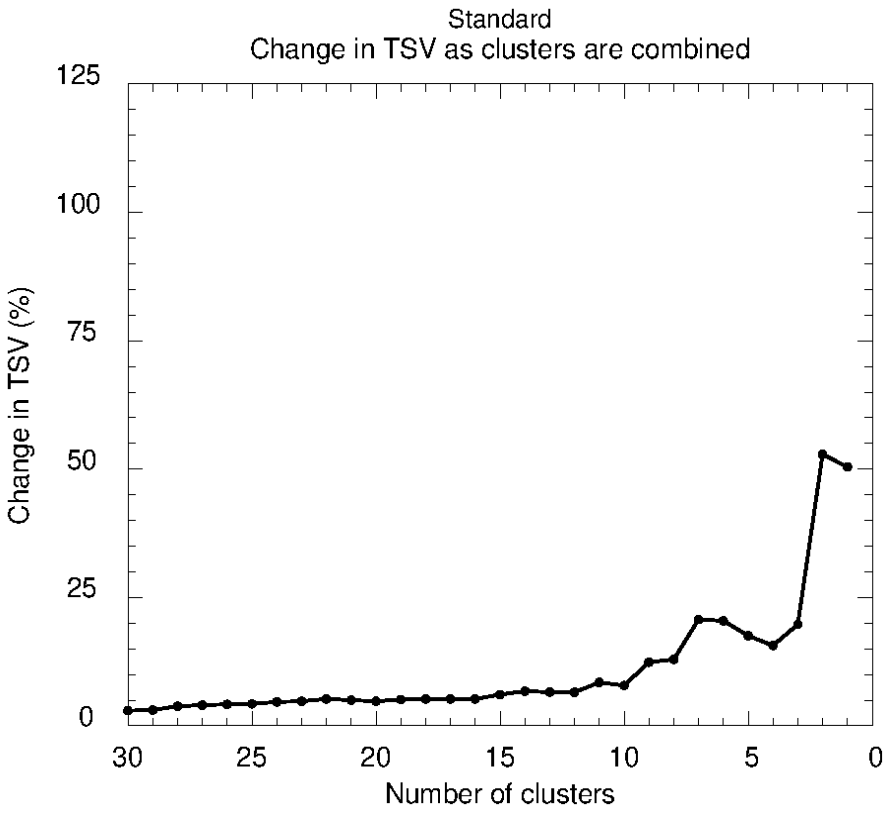

Figure A21: Total spatial variance for cluster analysis in the 2003-2004 neutral wet season

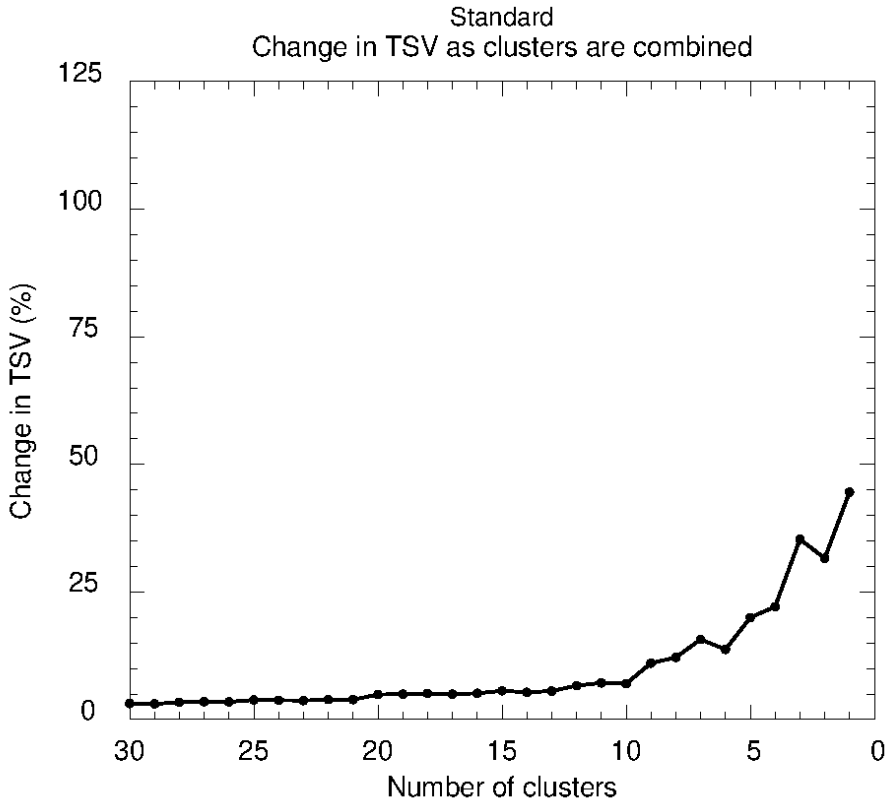

Figure A22: Total spatial variance for cluster analysis in the 2007-2008 La Niña wet season

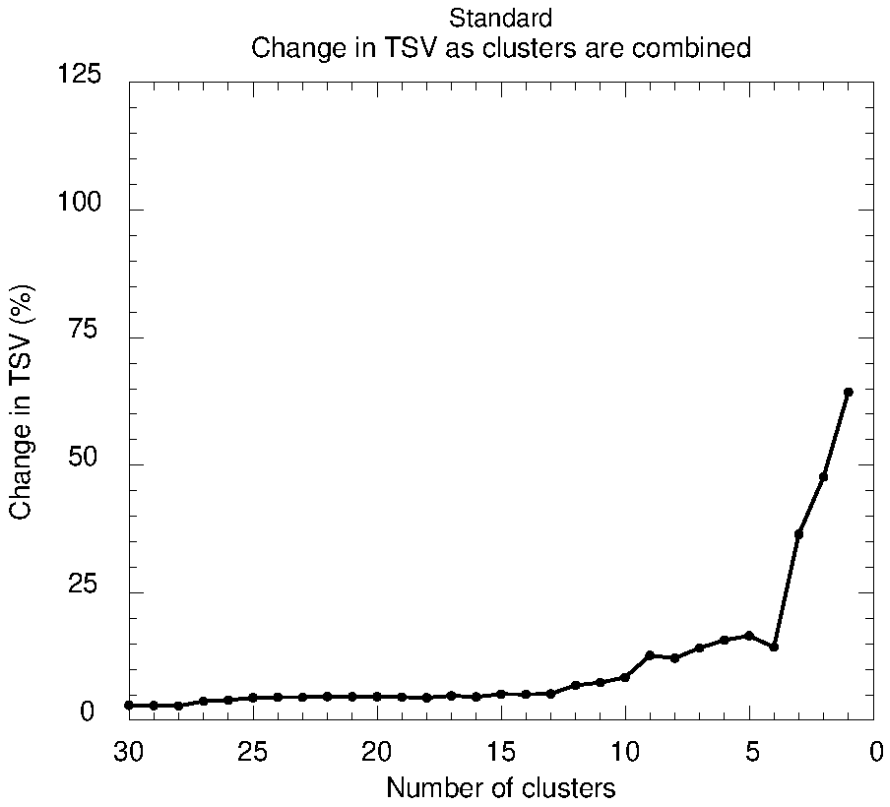

Figure A23: Total spatial variance for cluster analysis in the 2009-2010 El Niño wet season

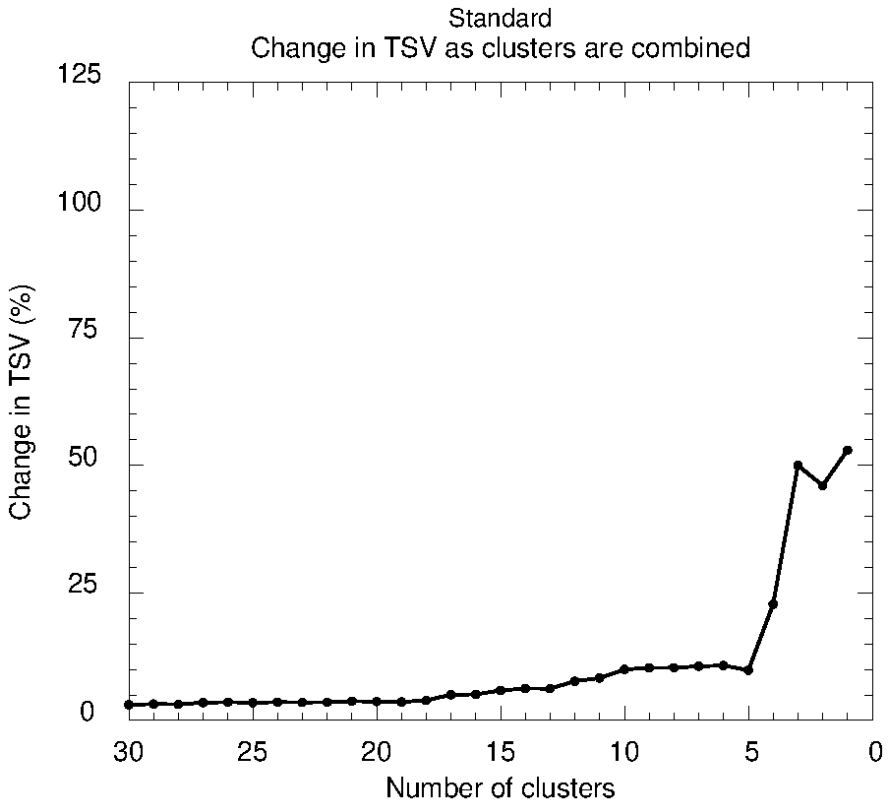

Figure A24: Total spatial variance for cluster analysis in the 2010-2011 La Niña wet season

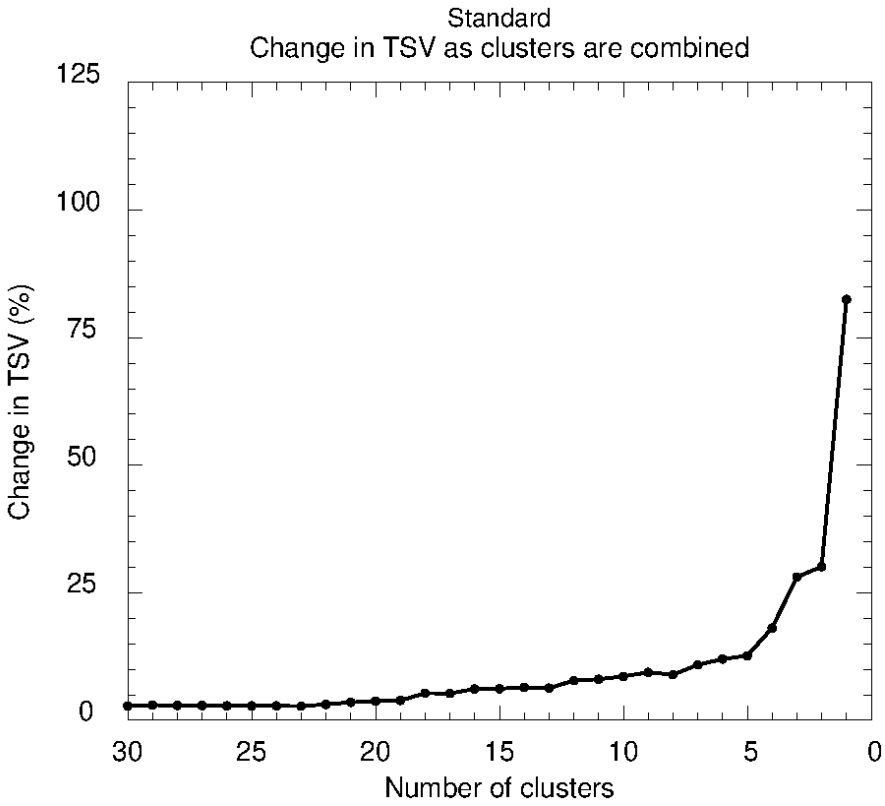

Figure A25: Total spatial variance for cluster analysis in the 2013-2014 neutral wet season

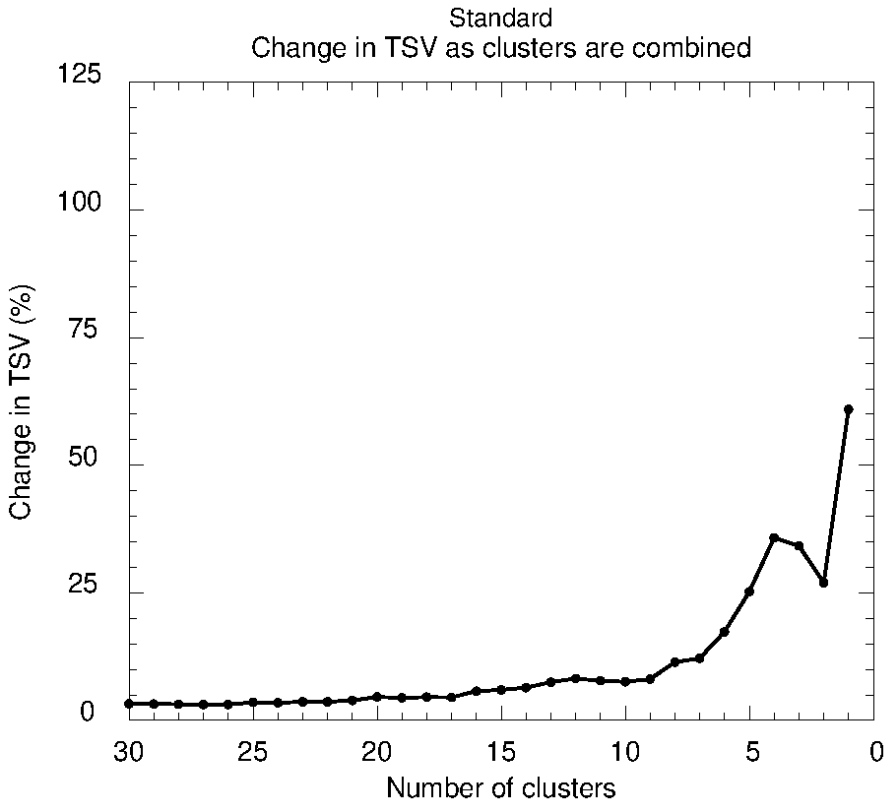

Figure A26: Total spatial variance for cluster analysis in the 2015-2016 El Niño wet season